# Diverse vase-shaped microfossils within a Cryogenian glacial setting in the Urucum Formation (Brazil)

L. Morais, B.T. Freitas, T.R. Fairchild, T.F. Toniolo, M.D.R. Campos, G.M.E.M. Prado, P.A.S. Silva, I.D. Rudnitzki, D.J.G. Lahr, J.M. Leme, et al.

▶ **To cite this version:**

L. Morais, B.T. Freitas, T.R. Fairchild, T.F. Toniolo, M.D.R. Campos, et al.. Diverse vase-shaped microfossils within a Cryogenian glacial setting in the Urucum Formation (Brazil). Precambrian Research, 2021, 367, pp.106470. 10.1016/j.precamres.2021.106470 . hal-03440852

**HAL Id: hal-03440852**
**https://hal.science/hal-03440852**

Submitted on 23 Nov 2021

**HAL** is a multi-disciplinary open access archive for the deposit and dissemination of scientific research documents, whether they are published or not. The documents may come from teaching and research institutions in France or abroad, or from public or private research centers.

L'archive ouverte pluridisciplinaire **HAL**, est destinée au dépôt et à la diffusion de documents scientifiques de niveau recherche, publiés ou non, émanant des établissements d'enseignement et de recherche français ou étrangers, des laboratoires publics ou privés.

# Diverse vase-shaped microfossils within a Cryogenian glacial setting in the Urucum Formation (Brazil)

L. Morais [a,b,*], B.T. Freitas [c,*], T.R. Fairchild [a], T.F. Toniolo [a], M.D.R. Campos [c], G.M.E.M. Prado [a], P.A.S. Silva [d], I.D. Rudnitzki [e], D.J.G. Lahr [f], J.M. Leme [a], P. Philippot [b,g], M. Lopez [g], R.I. F. Trindade [b]

[a] *Institute of Geosciences, University of São Paulo, Rua do Lago, 562, Cidade Universitária, CEP: 05508-080 São Paulo, Brazil*
[b] *Department of Geophysics, Institute of Astronomy, Geophysics and Atmospheric Sciences, University of São Paulo, Rua do Matão, 1226, Cidade Universitária, CEP: 05508-900 São Paulo, Brazil*
[c] *Geology Lab, School of Technology, University of Campinas, Rua Paschoal Marmo, 1888, Jardim Nova Italia, CEP: 13484-332 Limeira, Brazil*
[d] *Postgraduate Program in Geology and Geochemistry, Institute of Geosciences, Federal University of Pará, Cathodoluminescence Laboratory, Rua Augusto Corrêa, s/n, CEP: 66075-110 Belém, Brazil*
[e] *Departament of Geology, Federal University of Ouro Preto – DEGEO/UFOP, Morro do Cruzeiro, s/n – Bauxita, CEP: 35400-000 Ouro Preto, Brazil*
[f] *Department of Zoology, Institute of Biosciences, University of São Paulo – USP, Rua do Matão, travessa 14, 101, Cidade Universitária, CEP: 05508-090 São Paulo, Brazil*
[g] *Géosciences Montpellier, CNRS-UMR 5243, Université de Montpellier, Place Eugène Bataillon, 34095 Montpellier, France*

A B S T R A C T

Vase-shaped microfossils (VSMs) attributed to testate amoebae occur globally in diverse assemblages in Tonian rocks. These microfossils have thus been considered a potential biostratigraphic tool, especially for the interval between 789 and 729 Ma. Here we report a diverse and well-preserved in situ VSM assemblage, including several taxa previously considered as Tonian, within glacially influenced deposits for which sedimentological data support a Cryogenian age. However, the more robust recent multi-proxy correlation proposed by Freitas et al. (2021) indicates a Marinoan age for the studied succession. Detrital zircon data provide a maximum depositional weighted mean age of 749 ± 3 Ma for the VSM-bearing, organic-rich, fine-grained deposits within the Marinoan sequence in the Urucum Formation. Nine taxa are described from the fine-grained deposits in the upper Urucum Formation, Jacadigo Group, Brazil: *Cycliocyrillium simplex*, *Bonniea dacruchares*, *Bonniea pytinaia*, *Bombycion micron*, *Limeta lageniformis*, *Palaeoarcella athanata*, *Trigonocyrillium horodyskii*, *Pakupaku kabin* and cf. *Taruma rata*. The discovery of well-preserved in situ VSMs attributable to specific Tonian taxa within a Cryogenian succession challenges previous thinking that these organisms disappeared from marine ecosystems at the end of the Tonian.

*Keywords:*
Neoproterozoic
*Cycliocyrillium simplex* assemblage
Jacadigo Group
Global glaciation
Cryochron

## 1. Introduction

Biostratigraphically relevant fossils ideally must have wide geographic distribution, and their appearance and disappearance must be confined to a short, well-defined interval of geologic time. Their habitats, possible triggers for their appearance and disappearance, and taphonomic processes involved in their preservation must all be considered to establish a fossil as an index-fossil (Knoll et al., 2006).

For the Neoproterozoic, vase-shaped microfossils (VSMs) attributed to testate amoebae (Schopf, 1992; Porter et al., 2003) have been suggested as a biostratigraphic tool for Tonian carbonate, shale, chert and phosphatic rocks (Knoll and Vidal, 1980; Porter et al., 2003; Riedman

*E-mail addresses:* luanamoraiss@usp.br (L. Morais), bernardotf@ft.unicamp.br (B.T. Freitas), trfairch@usp.br (T.R. Fairchild), thiago.freitas.toniolo@gmail.com (T.F. Toniolo), marcelo.drdc@gmail.com (M.D.R. Campos), gustavo.marcondes.prado@usp.br (G.M.E.M. Prado), pedrogeologia8@hotmail.com (P.A.S. Silva), idrgeo@gmail.com (I.D. Rudnitzki), dlahr@ib.usp.br (D.J.G. Lahr), leme@usp.br (J.M. Leme), pascal.philippot@umontpellier.fr (P. Philippot), michel.lopez@gm.univ-montp2.fr (M. Lopez), ricardo.trindade@iag.usp.br (R.I.F. Trindade).

et al., 2018; Morais et al., 2019; Alvarenga et al., 2019), because, until now, nearly all VSM species have been reported solely from Tonian rock units: Kwagunt Formation, USA (Porter et al., 2003; Morais et al., 2019); Callison Lake Formation, Canada (Strauss et al., 2014; Cohen et al., 2017; Riedman et al., 2018; Morais et al., 2019); Visingsö Group, Sweden (Knoll and Vidal, 1980; Martí Mus and Moczydowska, 2000; Moczydłowska et al., 2018; Riedman et al., 2018); Ryssö Formation, Svalbard (Knoll and Calder, 1983; Riedman et al., 2018); Eleonore Bay Group, Greenland (Vidal, 1979; Green et al., 1988; Riedman et al., 2018); Togari Group, Tasmania (Saito et al., 1988; Riedman et al., 2018); Draken Formation, Svalbard (Knoll et al., 1991; Riedman et al., 2018); Elbobreen Formation, Svalbard (Martí Mus, 2001); Backlundtoppen Formation, Svalbard (Knoll et al., 1989; Riedman et al., 2018), Kingston Peak Formation, USA (Corsetti et al., 2003), Beck Spring Dolomite Formation, USA (Smith et al., 2015) and Chichkan Formation, Kazakhstan (Sergeev and Schopf, 2010). A rich and well-preserved VSM assemblage has also been reported in dolostone clasts near the base of the Neoproterozoic Urucum Formation, Jacadigo Group, Brazil (Fairchild et al., 1978; Morais et al., 2017). Because the source of these clasts was unknown until recently (see Freitas et al., 2021), a late Tonian age was suggested for these clasts (Morais et al., 2019) on the strength of the apparent biostratigraphic restriction of these VSM-bearing units to the upper Tonian. As Tonian carbonates have never been identified in the region of the Jacadigo Basin (*sensu* Freitas et al., 2011) on the southeastern Amazon Craton (e.g. Lacerda Filho et al., 2006), the Tonian source of the carbonate clasts was assumed to have been eroded away (Morais et al., 2019). In a similar manner, identification of the VSM Bonniea dacruchares Porter et al., 2003 has also been cited to corroborate stable isotope evidence for a Tonian age for another Brazilian stratigraphic unit, the Vazante Group on the São Francisco Craton (Alvarenga et al., 2019), even though the two specimens in palynological residues are three to four time smaller (15 and 25 μm in length) than the smallest previously reported specimen of this species (65 to 180 μm in length, e.g. Porter et al., 2003; Riedman et al., 2018; Morais et al., 2019; this study).

Here we describe the first occurrence of diverse well-preserved VSMs from newly discovered organic-rich fine-grained deposits clearly within the Urucum Formation itself, provide a new geochronological constraint for the age of the VSM-bearing succession of the Urucum Formation, and discuss the environmental, chronologic, and biostratigraphic implications of the new findings.

## 2. Geological setting

VSMs have been found in clasts (Fairchild et al., 1978; Morais et al., 2017; Morais et al., 2019) and now in beds of dolostone (Freitas et al., 2021) in the Urucum Formation, of the virtually unmetamorphosed and little deformed Jacadigo Group, in the Urucum mining district at Corumbá, Mato Grosso do Sul (MS), Brazil (Freitas et al., 2011; Trompette et al., 1998; Urban et al., 1992(Almeida, 1946); Fig. 1). The Urucum district is characterized by tabular hills rising many hundreds of meters above the Pantanal floodplains, named, from west to east, the Jacadigo, Tromba dos Macacos, Urucum, Santa Cruz, and Rabicho hills (Fig. 1B, C). All consist of a basal predominantly siliciclastic succession overlying, in erosional nonconformity, granite and metamorphic basement rocks of the 1.6 to 1.9 Ga Rio Apa Block (Lacerda Filho et al., 2006; Redes et al., 2015) and a thick upper part, mostly of iron formation (Lisboa, 1909; Dorr, 1945; Almeida, 1946; Barbosa and Oliveira, 1978; Urban et al., 1992; Freitas et al., 2011; Angerer et al., 2016; Fig. 1B, C).

Until recently, the Urucum Formation was described as siliciclastic,

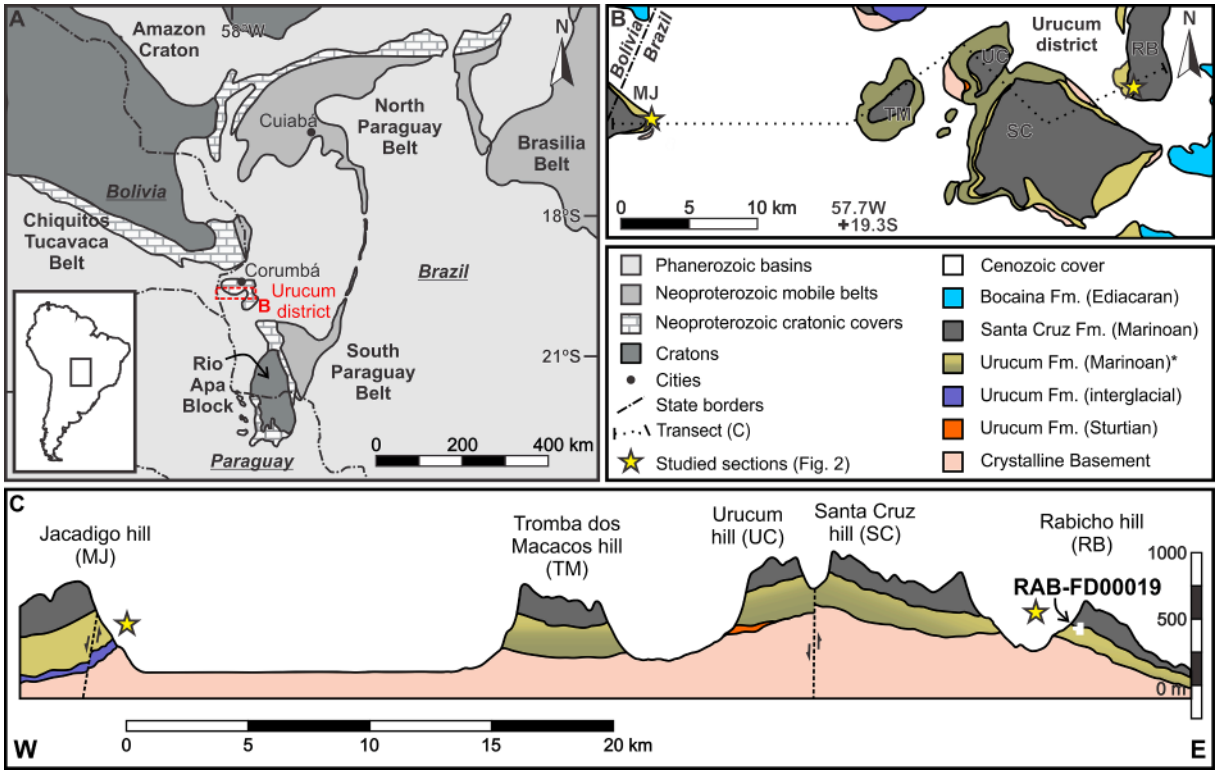


**Fig. 1.** Simplified map of the Urucum district and adjacent areas after Freitas et al., 2021. (A) Regional geological setting centered upon the Northern (NP) and Southern (SP) Paraguay Belt. Study area represented by the rectangle near Corumbá and detailed in B. (B) Simplified geologic map of the study area near Corumbá and approximate locations of the studied sections (stars). Easternmost star, location of drill core RAB-FD00019 (Fig. 2); westernmost star, location of studied succession at Jacadigo hill and the sample (Fig. 2; coordinates 411703 m E, 7874863 m S, 21 K) that furnished detrital zircon for geochronological analyses. (C) Schematic geologic cross-section of the Urucum district (after Freitas et al., 2021; Barbosa and Oliveira, 1978; Weiss and Sweet, 1959). Vertical scale, in meters above sea level. *Color transition represents deposits with (top) and without (bottom) ice-rafted clasts (after Freitas et al., 2021).

made up predominantly of arkosic sandstone, conglomerate, and breccia, with minor intercalations of diamictite, shale, and carbonate (e.g. Weiss and Sweet, 1959; Barbosa and Oliveira; 1978; Urban et al., 1992; Freitas et al., 2011; Angerer et al., 2016). It has been variously interpreted as representing lacustrine, fluvial, alluvial fan and fan delta continental depositional systems (Dorr, 1945; Almeida, 1946; Freitas et al., 2011), with some authors suggesting a glacial influence upon sedimentation as responsible for the diamictites and the abundance of outsized angular clasts within sandy facies (Dorr, 1945; Barbosa and Oliveira, 1978; Walde et al., 1981). Carbonate deposits were reported by Barbosa and Oliveira (1978) at the base of Jacadigo hill several decades after the descriptions in the 1940's (Alm(Almeida, 1945)eida, 1945; Almeida, 1946; Dorr, 1945) but were not mentioned again until very recently (Freitas et al., 2021). Barbosa and Oliveira (1978) described the Jacadigo hill succession as comprising, from base to top, marls with a carbonate intercalation, interspersed arkose and breccia with up to meter-scale carbonate clasts, fine-grained deposits, sandstone, and iron formation-dominated deposits (Fig. 2). Beneath the iron formations at Jacadigo hill, Urban et al. (1992) reported the occurrence of a sandstone and a "black shale" succession, from top to bottom of an unpublished drill core (Fig. 2).

Overlying the Urucum Formation the up to 400 m thick Santa Cruz Formation, composed mostly of banded iron formation, with minor Mn ore beds and siliciclastic intercalations, including diamictite, arkose and shale (Dorr, 1945; Almeida, 1946; Freitas et al., 2011), has been interpreted as glaciomarine deposits (Urban et al., 1992; Angerer et al., 2016). The age of this iron-bearing succession is constrained between 695 ± 17 Ma (youngest detrital zircon U-Pb age, Frei et al., 2017) and 587 ± 7 Ma (Ar-Ar burial heating age, Piacentini et al., 2013). This age range lends support to the idea that the lonestones within the iron formation may have originated during Cryogenian global glaciation. Indeed, two glacially influenced intervals, each followed by post-glacial carbonate successions, were recently recognized within the Jacadigo Group (Freitas et al., 2021). These sedimentary sequences were correlated with both Neoproterozoic cryochrons (Freitas et al., 2021). The new sedimentologic, stratigraphic, provenance and chemostratigraphic data presented by Freitas et al. (2021) reveal Sturtian continental glacial deposits underlying more than 600 m of transgressive carbonate deposits formed during the Cryogenian interglacial interval. Coarse-grained breccia, diamictite and correlative glacial outwash delta deposits displaying carbonate clasts eroded from the interglacial carbonate platform evidence Marinoan glacio-eustatic fall (Freitas et al., 2021; Fig. 2). Subsequent deposition of the transgressive iron formation-dominated succession of the Jacadigo Group (Figs. 1 and 2) is related to the Marinoan global glaciation collapse (Freitas et al., 2021).

We describe here fossils found in situ in organic-rich fine-grained deposits in drill core RAB-FD00019 (stored at the Institute of Astronomy and Geophysics of the University of São Paulo) that occurs near the top

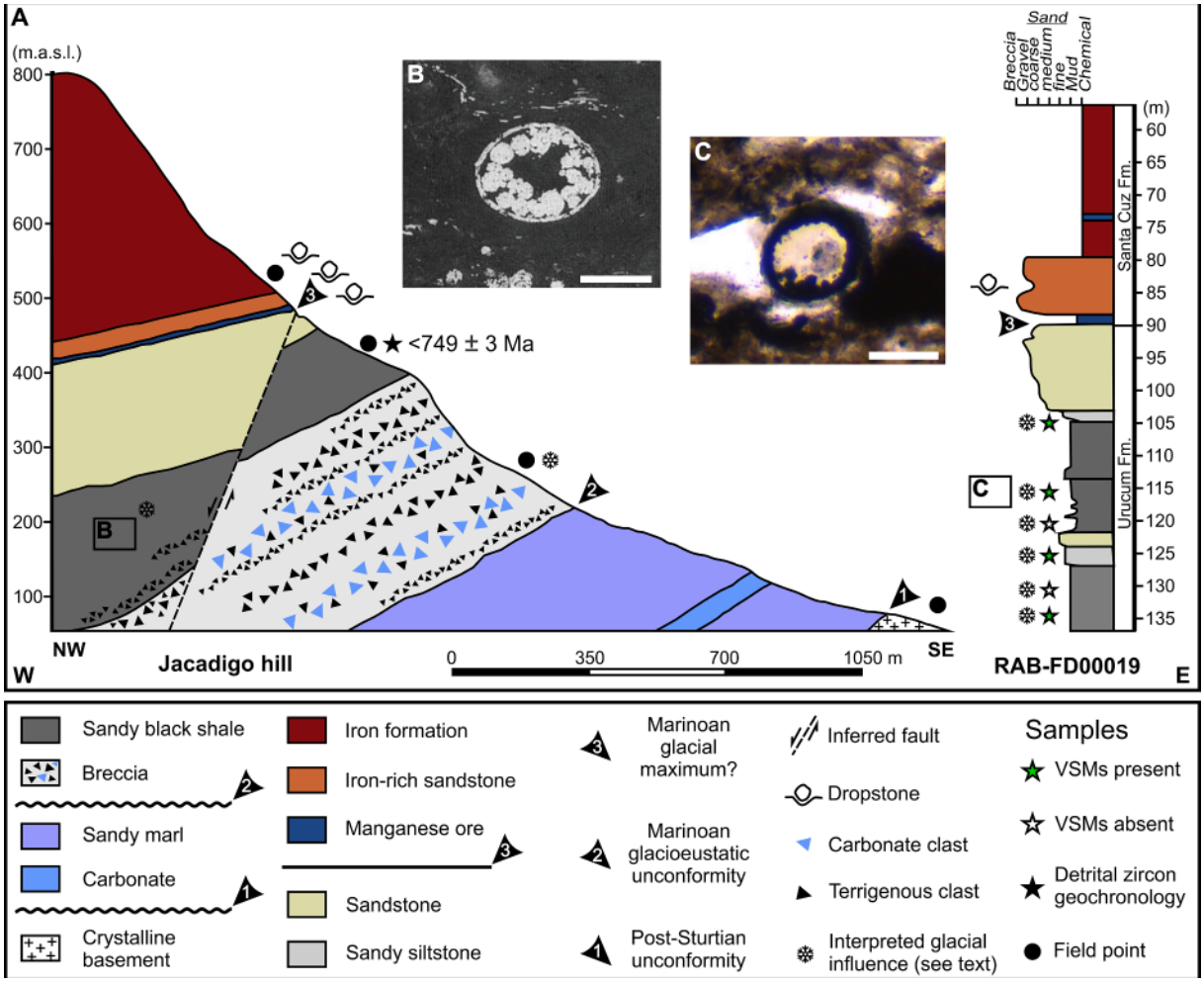


**Fig. 2.** Studied sedimentary successions and stratigraphic correlation (after Freitas et al., 2021) at: Jacadigo hill, as reconstructed from descriptions by Barbosa and Oliveira (1978) and Urban et al. (1992) (left); and at Rabicho hill, based on the description of the RAB-FD00019 core (right). (B) Photomicrograph from Urban et al. (1992) of unnamed circular structure partially filled by pyrite in the Jacadigo hill "black shale" succession. Scale bar: 25 μm. (C) Transverse section of VSM from the organic-rich fine-grained succession at Rabicho hill, described here. Scale bar: 50 μm.

of the Urucum Formation, within the Marinoan sequence (Freitas et al., 2021), at Rabicho hill in the eastern Urucum district. In situ VSMs are also reported from similar facies within the Marinoan sequence at Jacadigo hill, ~35 km to the west (Figs. 1 and 2).

## 3. Material and methods

The VSMs reported here were found in four of six thin sections made at the Instituto de Geociências at the Universidade de São Paulo (USP) of samples of organic-rich fine-grained deposits in drill core RAB-FD00019 (Fig. 2), three of which were used to study the systematics of this new VSM occurrence in the Urucum Formation: GP/5E-4373 from 104.90 to 105.00 m depth, GP/5E-4374 from 115.40 to 115.52 m depth, and GP/5E-4375 from 125.10 to 125.20 m depth, as measured from the top of the core (Fig. 2; Table 1). The VSMs were examined in ~50 μm-thick petrographic thin sections using a Leica DM 750 P microscope equipped with a Leica MC 170 HD camera at the Laboratório de Estudos Paleobiológicos at USP. Length (L), width (W), aperture diameter (AD) and neck length (NL) of the VSMs were measured according to Porter et al. (2003) (Table 1).

For palynological preparations, about 100 g of fresh rock from the six sampled intervals of the RAB-FD00019 core were dissolved in HCl (36%) for two days and then rinsed repeatedly with distilled water. After neutralization, the residues were placed in HF (40%) for one day and again rinsed repeatedly with distilled water. VSMs favorable for taxonomic identification were physically separated from the residue under a binocular microscope. Individual microfossils were submitted to LEO 440 scanning electron microscopy, energy dispersive spectroscopy and X-ray Dispersive Energy (EDS), at the Centro de Pesquisas Geocronológicas (CPGeo-USP). Raman spectroscopy was carried out at the Brazilian Research Unit of Astrobiology (NAP/Astrobio) using a Renishaw inVia micro-Raman, with 532 nm excitation wavelength; spectra were collected with a 50X objective. See supplementary online material (SOM 1; 2) for details.

Duplicate thin sections of the samples from the RAB-FD00019 core studied for microfossils were prepared at the Universidade Federal do Pará (UFPA) for microfacies analysis. Six ~35 μm-thick, polished petrographic thin sections were imaged using reflected and transmitted light, as well as cathodoluminescence (CL). Images were obtained in the Laboratório de Catodoluminescência at UFPA using a Leica DM 4500 P LED coupled with a Leica DMC camera and a CL 8200 Mk5-2 device. CL data were acquired with an electron beam current of 260 to 384 μm, constant acceleration voltage of 15.5 kV, and 12.5 to 18.0 s exposure time.

Zircon grains for geochronologic analysis were obtained from an outcrop sample of the VSM-bearing, organic-rich, fine-grained succession at Jacadigo hill (411703 m E, 7874863 m S, 21 K) , equivalent stratigraphically and facies-wise (Lisbo(Lisboa, 1909)a, 1909; Almei (Almeida, 1946)da, 1946; Urban(Urban et al., 1992) et al., 1992) (Figs. 1 and 2) to samples examined from the RAB-FD00019 core from Rabicho hill, ~35 km to the east (Freitas et al., 2021). Sample preparation and age-dating were carried out at the Instituto de Geociências at the Universidade Estadual de Campinas. Zircon grains, separated from the rock sample using standard density and magnetic methods, were arbitrarily handpicked under a microscope and fixed in an epoxy resin disc that was ground and polished to expose each zircon grain in cross section.

Single grain isotopic analysis was done using an Excite193 laser ablation system (Photon Machines), equipped with a two-volume HelEx ablation cell, coupled to an ICP-MS Element XR (Thermo Scientific). Beam diameter was set to 25 μm and acquisition time, 40 s. Isotopic ratios were checked using the standards 91,500 (Wiedenbeck et al., 1995) and PEIXE (Navarro et al., 2017). See Navarro et al. (2015) for further information on the analytical routine. Data processing utilized the Software Iolite 2.5 following the method proposed by Paton et al. (2010). Error Correlations (Rho) were calculated considering $^{207}Pb/^{235}U$ and $^{206}Pb/^{238}U$ isotopic ratios using the equation given by Schmitz and Schoene (2007).

Only ages with concordance greater than 90% and reverse discordance lower than 110% were considered in this study. Common lead correction was not made because $^{204}Pb$ signals were low in virtually all grains. Zircon grains with anomalous $^{204}Pb$ concentrations were

**Table 1**
Morphometric parameters of vase-shaped microfossils from the Urucum Formation. n = number of specimens.

| Study | Level (m) | Specie | L/W (n) | Length (L) (μm) | Width (W) (μm) | Neck-length (μm) | Aperture (μm) |
|---|---|---|---|---|---|---|---|
| Urucum Fm. (RAB-FD00019, this study) | 115.40–52 | *Bonniea dacruchares* | 1.3–2.0 (21) | 49–159 | 29–106 | – | – |
| | 115.40–52 | *Bonniea pytinaia* | 1.3–2.2 (5) | 134–166 | 62–103 | – | – |
| | 115.40–52; 125.10–20 | *Bombycion micron* | 1.5–1.7 (4) | 88–196 | 57–130 | – | 17–65 |
| | 104.9–105; 115.40–52; 125.10–20 | *Cycliocyrillium simplex* | 1.2–1.3 (4) | 134–181 | 77–119 | – | – |
| | 115.40–52 | *Limeta lageniformis* | 1.8–2.6 (2) | 137–213 | 76–82 | 50–85 | – |
| | 115.40–52 | *Palaeoarcela athanata* | 0.2–0.5 (4) | 28–47 | 78–138 | – | 90 |
| | 115.40–52 | *Trygonocyrillium horodiskii* | 1.0–1.2 (3) | 72–84 | 68–80 | – | – |
| | 115.40–52 | cf. *Taruma rata* | 0.83–1.31 (2) | 89–103 | 68–124 | – | – |
| | 115.40–52; 125.10–20 | *Pakupaku kabin* | 1.5–1.6 (2) | 89–148 | 53–97 | – | 25–27.7 |
| Urucum Fm. (Morais et al., 2017; Morais et al., 2019) | Dolomitic clasts in diamictite near the base of the succession at Rabicho hill | *Bonniea dacruchares* | 1.4–1.3 (2) | 65–88 | 46–65 | – | 15–23 |
| | | *Cycliocyrillium simplex* | 1.0–1.8 (24) | 50–139 | 42–96 | – | 11–37 |
| | | *Cycliocyrillium torquata* | 1.2–1.5 (10) | 53–113 | 40–84 | 3–18 | 12–34 |
| | | *Limeta lageniformis* | 1.5–2.0 (10) | 100–133 | 50–70 | 20–59 | 12–32 |
| | | *Palaeoamphora urucumense* | 1.2–1.7 (6) | 90–135 | 60–109 | 11–19 | 38–66 |
| | | *Taruma rata* | 1.2–1.4 (3) | 91–94 | 65–73 | – | 17–21 |
| | | *Trygonocyrillium horodiskii* | (1) | – | – | – | 20 |

– impossible to measure.

excluded from the analysis. Ages older than 1000 Ma were established using the $^{207}Pb/^{206}Pb$ isotopic ratio and ages younger than 1000 Ma by the $^{206}Pb/^{238}U$ ratio. This value is within the minimum of 800 Ma and maximum of 1500 Ma for cutoff values commonly used in detrital zircon geochronology (e.g. Babinski et al., 2013; Spencer et al., 2016; Vermeesch, 2021). Ages are given with 2σ uncertainties.

The RAB-FD00019 drill core is stored at the Instituto de Astronomia e Geofísica, USP, Brazil. Petrographic thin sections analyzed here are deposited in the Laboratório de Paleontologia Sistemática (LPS) of the Instituto de Geociências, USP, Brazil.

## 4. Results and discussion

### 4.1. Sedimentary successions

The 136.6 m-long RAB-FD0019 drill core recently recovered from Rabicho hill in the eastern Urucum district (Figs. 1 and 2) samples nearly 50 m of fine-grained siliciclastic deposits overlain conformably by almost 90 m predominantly of iron formation, with subordinate intercalations of manganese ore (Fig. 2). This same stratigraphic relationship is recognizable throughout the Urucum district, where tabular hills have the lower section ascribed to the Urucum Formation siliciclastic succession, named after the Urucum hill (Almeida, 1946), and the upper iron-rich deposits to the Santa Cruz Formation, named after the Santa Cruz hill (Almeida, 1946), the two comprising the Jacadigo Group, named after the Jacadigo hill (Almeida, 1946) (Figs. 1 and 2).

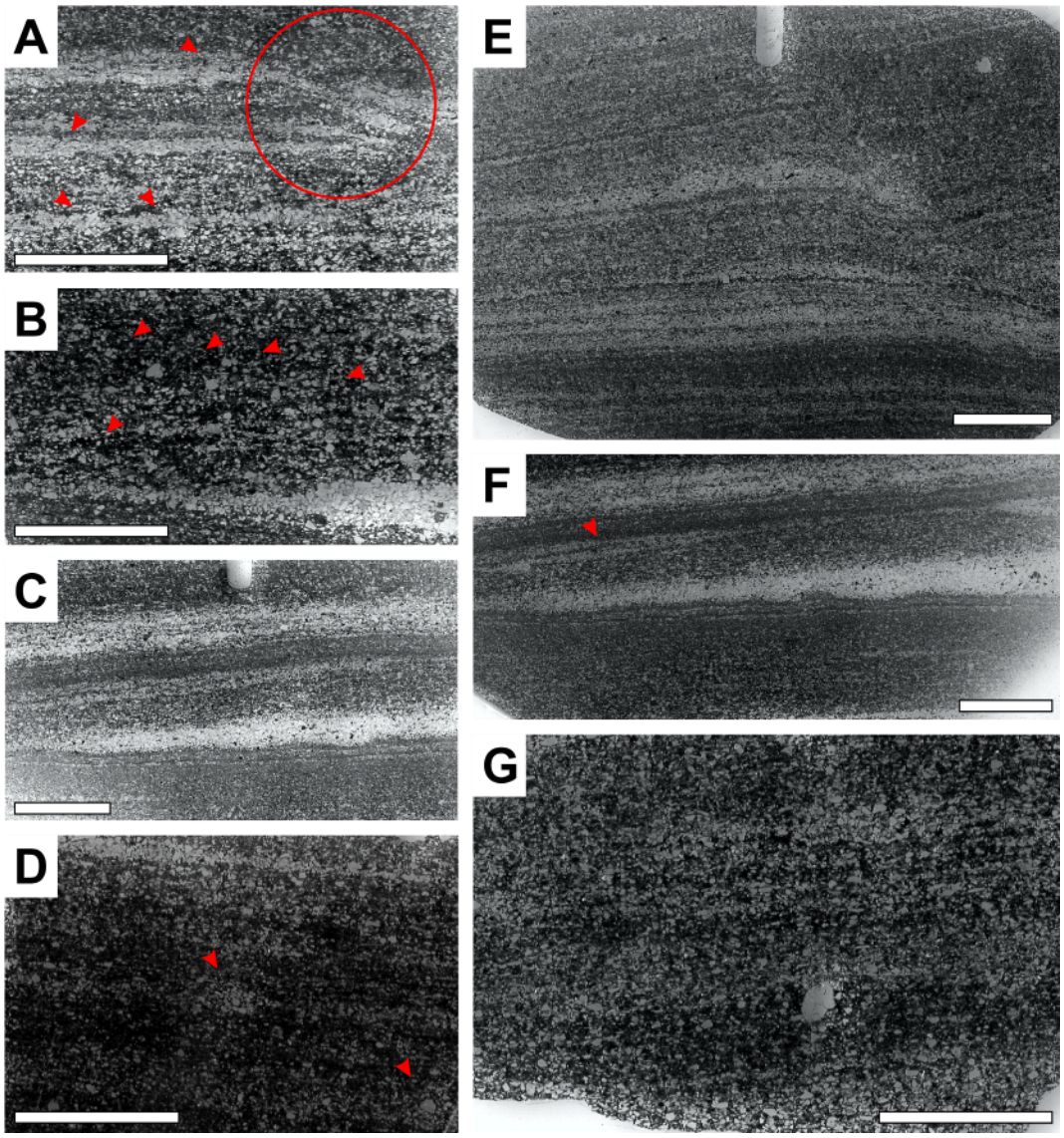


**Fig. 3.** VSM-bearing facies from the RAB-FD00019 core in partial views of thin sections from the sampled levels identified by approximate depth below the surface. (A) 105 m depth. Poorly sorted, coarser portion of thin section displaying sand-dominated sub-horizontal laminae, with grain clusters (red arrows) and deformed laminae (red circle), and minor intercalations of organic-rich mud. (B) 105 m depth. Finer part of same thin section displaying wispy lamination with poorly sorted angular to subangular sand grains. Note the lensoidal cluster of sand grains at lower right and dispersed circular alignments of silt and sand grains around black mud (red arrows). (C) 115 m depth. Laminated aspect of the sandy, organic-rich, fine-grained deposits bearing VSMs. Note the poorly defined limits between coarser and finer sediments. (D) 120 m depth. Facies like that in B. Note the common occurrence of circular grain alignments, locally concentric (red arrows). (E) 125 m depth. Facies like that in C. Note *syn*-sedimentary deformation at right. (F) 130 m depth. Facies like that in C. Note sub-horizontal and inclined (red arrow) orientations of framework and matrix components (G) 134 m depth. Facies like that in B and D with isolated and fractured coarse sand grain. Scale bars: 5 mm. (For interpretation of the references to color in this figure legend, the reader is referred to the web version of this article.)

Most of the sedimentary successions at Jacadigo, Urucum, Santa Cruz and Rabicho hills occur above the Marinoan glacio-eustatic unconformity recognized by Freitas et al. (2021; Figs. 1 and 2).

The lower 30 m of the RAB-FD0019 drill core is laminated, carbonate-cemented black shale with thin wispy siltstone to very-fine sandstone laminae (Fig. 3A–G) and at mid-section 4.5 m of fine grey sandstone, locally displaying asymmetrical ripples (Fig. 2B). This shaley facies grades upward into a 16 m thick altered medium to coarse sandstone with a sharp change in color from medium grey to yellowish-orange three meters above its base. This sandstone interval is abruptly capped by a meter-thick layer of manganese ore (including braunite and cryptomelane – Fig. 2B) recognized regionally as the base of the Santa Cruz Formation (Walde et al., 1981; Urban et al. 1992). Continuing upward, a 7 m-thick hematite-cemented arkose displaying outsized lonestones, is followed by massive to laminated hematite-jaspilite ironstone containing a second prominent meter-thick intercalation of manganese ore (Fig. 2B).

Black shales in the Urucum Formation are also found at Jacadigo hill, some 35 km west of the site of the RAB-FD00019 drill core (Figs. 1 and 2). Based on the description of a drill core studied by Ananiadis (1984), Urban et al. (1992) reported more than 100 m of "black shales and black siltstones with some coarse-grained clastic intercalations" below the uppermost sandstone succession topping the Urucum Formation. Interestingly, one of their figures (Urban et al. 1992; Fig. 10F), a photomicrograph of the Jacadigo hill "black shale" (Fig. 2B), clearly illustrates a pyritized test indistinguishable from VSMs from the RAB-FD00019 core shown here (Fig. 2C).

The stratigraphic section at Jacadigo hill was previously described as comprising, from bedrock upward, sandy marls with an intercalated carbonate bed, boulder-grade breccia intercalated with coarse-grained arkose, organic-rich fine-grained deposits, sandstone, Mn-rich beds and an iron formation-dominated succession (Barbosa and Oliveira, 1978; Urban et al., 1992; Fig. 2). Our investigation of the Jacadigo hill escarpment confirmed the occurrence of outcrops of crystalline basement rocks, boulder-grade breccia, fine-grained siliciclastic facies and the iron-formation succession (Fig. 2).

The breccia is poorly sorted, polymictic, boulder-grade, with up to meter-scale carbonate clasts (Fig. 4A), locally displaying preserved faceted and striated granite clasts (Fig. 4B), as well as tabular intraformational conglomeratic sandstone pebbles, cobbles, and boulders. A deeply weathered exposure of the fine-grained facies (coordinates 411703 m E, 7874863 m S, 21 K), correlatable to that reported by Urban et al. (1992) in the limited area of the Jacadigo hill (Figs. 1 and 2), was sampled for geochronological analysis of detrital zircon. The iron formation-dominated succession of the Santa Cruz Formation presents isolated outsized clasts, including a meter-scale boulder composed of diamictite (Fig. 4C).

Not only are they remarkably similar in stratigraphy, but the sedimentary successions studied at Rabicho and Jacadigo hills also display the same structural trends dominated by gentle deformational patterns typical of all the Urucum district (Fig. 1C), indicating that they are not far-travelled allochthonous structural blocks or olistoliths. The Urucum Formation has long been described as dominated by sandstone and coarse-grained facies with minor shale deposits based on discontinuous sections in the center of the Urucum district and on continuous, but thinner successions up to 100 m thick at the borders of the district (e.g. Almeida, 1946; Barbosa and Oliveira, 1978; Freitas et al., 2011). The two shale-dominated successions revealed in drill cores provide the only known continuous stratigraphic record of the Urucum Formation where the unit is thicker. Previous detailed facies analysis of the Urucum Formation (Freitas et al., 2011) did not have access to such continuous sections of the formation in any of the major hills of the Urucum district. Study of the drill cores and our recent field work thus indicate that dominantly fine-grained successions are probably more common in the Urucum Formation than previously thought (see Freitas et al., 2021 for detailed stratigraphy and sedimentary evolution of the Jacadigo Group).

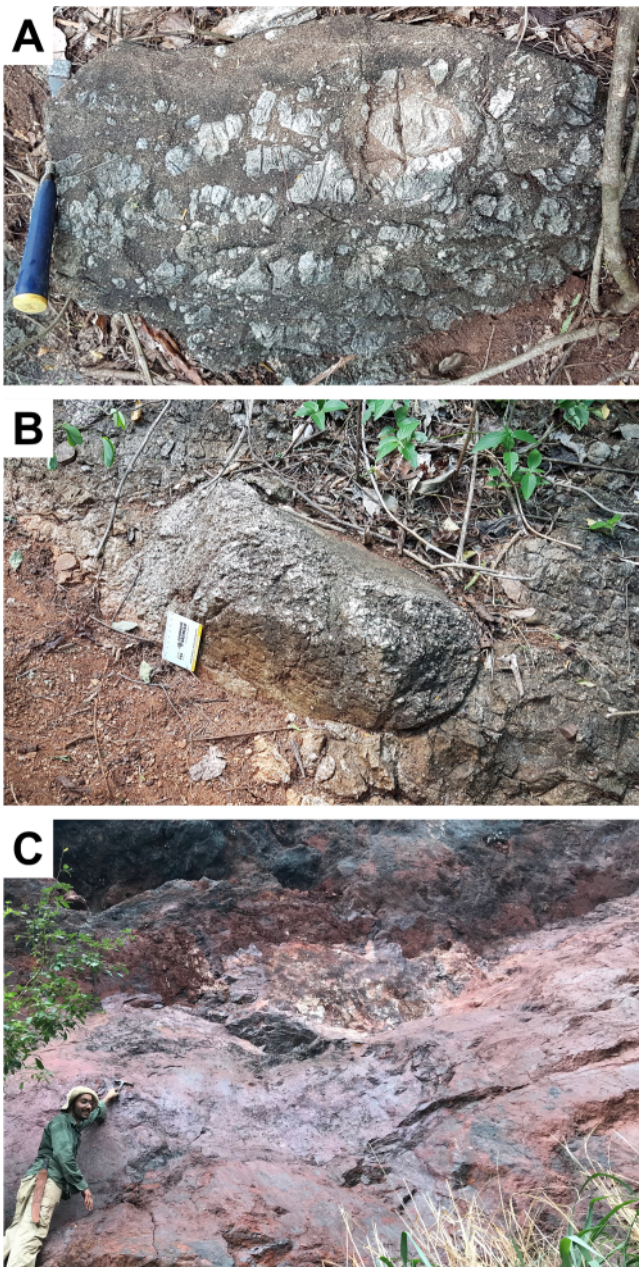


**Fig. 4.** Examples of the sedimentary facies recognized at Jacadigo hill. (A) Poorly sorted sand to cobble-grade framework of polymictic breccia with abundant carbonate clasts. (B) Faceted and striated granite boulder within poorly sorted sandy breccia. (C). Meter-scale diamictite boulder deforming underlying sub-horizontal bedding in iron formation.

### 4.2. *Microfacies of VSM-bearing fine-grained successions*

The six studied thin sections from the RAB-FD00019 core display 15 to 40% matrix content and thus can be classified as lithic wacke (Dott, 1964) (Fig. 3; Fig. 5A, B). Aluminum and ferroan clay minerals are present in the matrix, as indicated by their dull, dark luminescence (Götze et al., 2002; Okamura et al., 2006), as well as dispersed clay to silt-size quartz, feldspar and carbonate grains, and incipiently to irregularly laminated amorphous brownish matter containing kerogen, as indicated by Raman spectroscopy (Fig. 5C–F).

The framework is made up of poorly sorted silt to sand grains that are dominantly very angular and rarely rounded (Fig. 5A, B). Grains are mainly quartz, microcline, plagioclase, chert, muscovite and lithic fragments, including carbonate and siliciclastic mudstone clasts, the

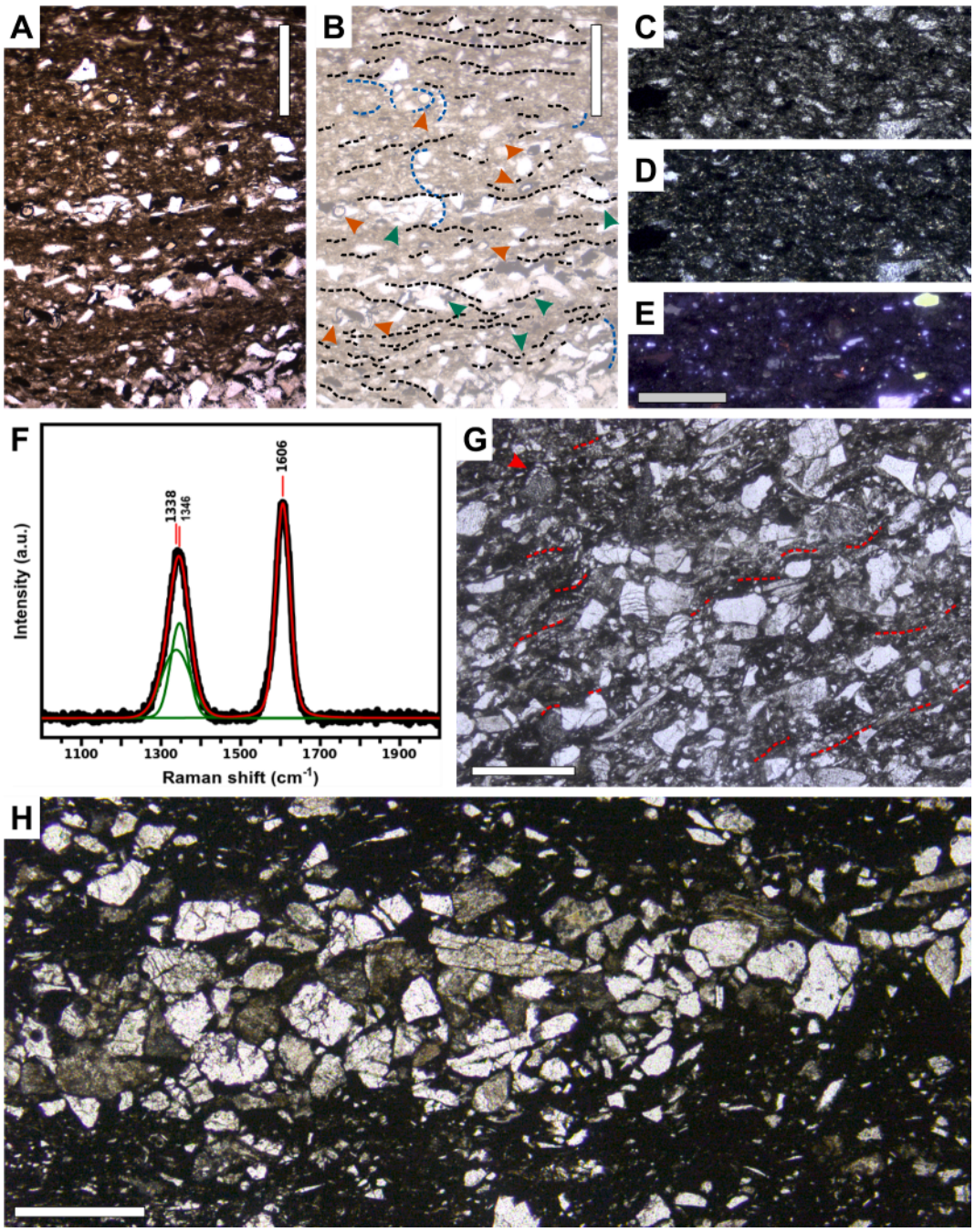


**Fig. 5.** Textural aspects and microfacies of the in-situ-VSM-bearing succession in drill core RAB-FD00019 from Rabicho hill. (A, B) Transmitted light photomicrograph of sample from ~115 m depth. Note dominance of poorly sorted scattered angular silt and sand grains, as well as sand clusters (green arrows), VSMs (orange arrows), crinkled anastomosed matrix fabric (black dashed lines), and semi-circular grain alignments (dashed blue lines). (C-E) Transmitted light (C), crossed Nicols (D) and cathodoluminescence images (E) of matrix in the same sample as in A and B. Note the crinkled matrix fabric, clay mineral (high birefringence in D) and dispersed poorly sorted angular silt to fine sand grains including grains of carbonate (orange luminescence in E) and plagioclase (green luminescence in E). (F) Raman spectra of brownish amorphous material with diagnostic peaks of kerogen. (G) Transmitted light photomicrograph showing abundant poorly sorted angular silt to coarse sand with many fractured grains and detrital mica at 104 m depth. Note thin silt coating on sand grain (red arrow) and incipient anastomosed matrix fabric (red dashed lines), despite the dominantly random clast orientations associated with clast clustering. (H) Relatively large irregular clast cluster under transmitted light. Note abundant fractured grains, as well as semi-circular grain alignments, at 120 m depth. White scale bar: 500 μm. Grey scale bar: 200 μm. (For interpretation of the references to color in this figure legend, the reader is referred to the web version of this article.)

latter locally observed as pseudomatrix. Silt and sand clasts are often triangular with serrated edges (Fig. 5A, B). Ten to thirty percent of the framework grains exhibit internal fractures (Fig. 5G, H). Grains with crescentic, curvilinear edges are observed locally.

Silt and quartz grains are often matrix-supported and may occur isolated, sparsely, or in irregular lensoidal clusters (Fig. 3; Fig. 5A–E, G, H). Macroscopic laminations (Fig. 3) are made up of these grain clusters (Fig. 5A, B, H) which form thin bands often less than 1 mm thick and up to a few millimeters long. Irregular clast clusters comprise between 10 and 40% of the analyzed thin sections. Circular clusters of clasts are also commonly observed, comprising 10 to 30% of the thin sections, and their abundance is directly proportional to matrix content. These

clusters are 20 to 840 μm in diameter, contain varied proportions of matrix and framework (Fig. 6A–F), commonly display a matrix-dominated inner part delineated by a circular alignment of silt and/or sand grains (Fig. 6A, B). Semi-circular, ellipsoidal and concentric grain alignments also occur (Fig. 3; Fig. 5A, B; Fig. 6A–F). The same arrangement has also been illustrated in the organic-rich fine-grained deposits at Jacadigo hill reported by Urban et al. (1992; Fig. 6G, H).

Complete VSM tests occur in both matrix- and framework-dominated microfacies, including the grain clusters described above (Fig. 5A, B), comprising around 5% of the four thin sections in which they were found. Broken tests are also present (Fig. 5A, B). Tests are incrusted by small pyrite crystals (about 11.4 μm mean diameter) (Fig. 7), but minor quartz and kerogen may also be present in the test-wall, as demonstrated by Raman spectroscopy (Fig. 7G, H). Clay mineral coatings locally occur on pyritized tests (Fig. 5A, B; Fig. 6G, H; Fig. 8D–F). Tests are usually filled by matrix, silica (Fig. 8A–F), pyrite (Fig. 5A, B; Fig. 6G, H; Fig. 7A, B; Fig. 8G, H) or, less commonly, carbonate (Fig. 8G, H). Organic-walled sphaeromorphic acritarchs are locally observed (Fig. 8I)

Although framework clasts are predominantly bounded by matrix material, syntaxial quartz and plagioclase overgrowths are common (Fig. 9A). Calcite can replace detrital grains, sometimes delineating grain clusters (Fig. 9B). μm-scale pyrite crystals are locally dispersed in the rock matrix around framework grains (Fig. 5A, B; Fig. 6G, H; Fig. 7A, B), but larger euhedral pyrite may also be observed (Fig. 7B). The rock matrix usually displays varied, often crinkled and anastomosed ductile fabrics, (Fig. 5A–E, G; Fig. 6C–F; Fig. 7B; Fig. 9A–D), even in the organic-rich facies at Jacadigo hill (Fig. 6G, H). Syn-sedimentary fault domains locally affect matrix fabrics and clast clusters (Fig. 3E; Fig. 9C, D).

### 4.3. Facies interpretations

The sedimentary succession preserved in the major hills of the Urucum district exhibits an overall change from siliciclastic-dominated sedimentation in the Urucum Formation to massive iron and manganese precipitation in the Santa Cruz Formation, however with evidence of glacial influence along both successions. This abrupt change in stratigraphy may represent a condensed record related to glacial maximum (Fig. 2) during the Marinoan global glaciation (Freitas et al., 2021).

The sedimentary features observed below (Fig. 3A, B) and above (Fig. 3C) the organic-rich fine-grained succession at Jacadigo hill (Fig. 2) display clear evidence of glacial transport. Meter scale clasts and striated boulders within the breccia unit at Jacadigo hill are interpreted as ice-rafted rock fragments. Intraformational tabular conglomeratic sandstone clasts and meter-scale diamictite clasts interpreted as dropstones of till most probably originated due to cementation by ice in a glacial context (e.g. Waller et al., 2009; Runkel et al., 2010; Chumakov, 2015).

The correlative upper successions of the Urucum Formation at both Rabicho and Jacadigo hills clearly display a coarsening-upward succession (Fig. 2) compatible with progradation of sediment feeding directly into a standing body of water. The textural characteristics of the fine-grained succession at the top of the Urucum Formation at Rabicho hill examined here are very similar to sediments produced under freeze-to-thaw cycles and by glacial erosion: angular grain shapes and variable grain relief have been widely recognized in modern glacial deposits (Sweet and Brannan, 2016; Mazumder et al., 2017; Hart, 2017; Yang et al., 2018). The same is true for fractured sand-grade grains, formed under subglacial deformation and frost weathering of unconsolidated sediment (e.g. Hiemstra and Van der Meer, 1997; Woronko and Pisarska-Jamroży, 2016).

Grain clusters like those found here are also described in recent glacially influenced settings (Hiemstra and Van der Meer, 1997; Hiemstra and Rijsdijk, 2003; Piotrowski et al., 2006; Kilfeather et al., 2010), where they are attributed to shearing, rotation and compaction below ice-streams or to thermal compaction related to water state changes within sediment (Cowan et al., 2012). Glacial shearing is also evidenced by the anastomosed and sub-horizontal matrix fabrics observed in the thin sections (Fig. 5A–E, G; Fig. 6A–H; Fig. 7B; Fig. 8D–F; Fig. 9A–D). These matrix fabrics resemble the plasmic microfabrics of Meer (1993), widely interpreted as incipient to fully developed shear planes in glacially deformed cohesive sediment (Kluiving et al., 1999; Hiemstra et al., 2005; Phillips et al., 2007; Kilfeather et al., 2010; Menzies and Meer, 2018). Additional framework and matrix relationships diagnostic of glacial deformation as synthesized by Meer (1993), can also be seen in the studied thin sections: discrete shear lines (Fig. 5A–E; Fig. 6A, B; Fig. 7A, B) and strain shadows and caps (Fig. 3A–G; Fig. 5A–E, G; Fig. 6C, D; Fig. 8D, E; Fig. 9C, D) described here as anastomosed and sub-horizontal matrix fabrics, silt and clay caps (Fig. 5A, B, G; Fig. 8D, E), crushed grains (Fig. 5G, H), faulted domains (Fig. 3E; Fig. 9E, F), and rotational structures (Fig. 3A, B, D, F, G; Fig. 5A, B, G, H; Fig. 6A–D; Fig. 7A, B; Fig. 8D, E; Fig. 9E, F).

Subglacial deformation features, high proportion of angular and fractured grains, and common occurrence of very-fine silt clasts, including plagioclase, indicate an ice-proximal setting (Sweet and Brannan, 2016; Menzies and Meer, 2018). The apparent lack of coarse pebbles and larger clasts in the studied interval suggest deposition of the fine-grained succession beneath an ice shelf between the grounding-line and the calving line (e.g. Domack et al., 1999; Fig. 10). Variations in the proportions of clast clusters along the organic-rich, predominantly fine-grained succession is tentatively interpreted as related to glacial advance and retreat (Fig. 10). This idea is consistent with the interpretation of the sandstone intervals at the top of the Urucum Formation (Fig. 10) as glacial outwash deposits following glacier retreat (Freitas et al., 2021). The abundance of kerogen and presence of acritarchs within the studied deposits indicates local primary productivity in this glacially influenced sedimentary environment. The diverse cements found filling tests as well as in the surrounding rock may reflect the varied chemical complexity of the sub ice shelf marine environment and later associated diagenetic fluids (e.g. Yang et al., 2018).

The predominance of well-preserved whole tests of fragile VSMs and presence of delicate organic-walled acritarchs argue against their transport over long distances and in favor of their origin as autochthonous elements that settled from suspension. Glacial deformation after deposition obliterated most primary sedimentary structures indicative of original hydrodynamic conditions associated with the entombment of the microfossils. Early diagenesis and preservation inside sediment clusters developed under glacial deformation of a frozen substrate must have spared microfossils from destruction.

Based on the above evidence and interpretations, we argue that the preserved tests do not represent reworked previously deposited microfossils transported to the depositional site but rather are from contemporary autochthonous to parautochthonous testate amoebae from the water column below the ice shelf and in adjacent open marine settings (Fig. 10). They may even have lived in cryoconite holes and pans developed on the surface of ice and connected to englacial and subglacial flow networks (e.g. Hoffman, 2016; Hawes et al., 2018). In fact, some grain clusters, especially concentric ones (e.g. Fig. 5A, B; Fig. 6E, F) are similar to modern cryoconite granules (e.g. Takeuchi et al., 2010; Hodson et al., 2010; Cook et al., 2016).

### 4.4. Maximum age of VSM-bearing fine-grained successions

The broadest age constraints for the rocks and microfossils studied here range between 1.9 and 1.7 Ga, the age of the local basement (Redes et al., 2015; McGee et al., 2018), and 587 ± 7 Ma, the age of anchimetamorphism recorded in the overlying Santa Cruz Formation (Piacentini et al., 2013). We carried out detrital zircon U-Pb analysis by laser ablation on 179 detrital zircon grains from the VSM-bearing, organic-rich, fine-grained succession of the Urucum Formation at Jacadigo hill. Of these, 79 yielded ages with concordance greater than 90% (Freitas et al., 2021; Fig. 11A, B; SOM 2, Table S5). Five grains were not considered because of apparent Pb loss (Fig. 11A; Table S5) (Andersen et al., 2019). Two peaks (local maxima) were identified in the Kernel

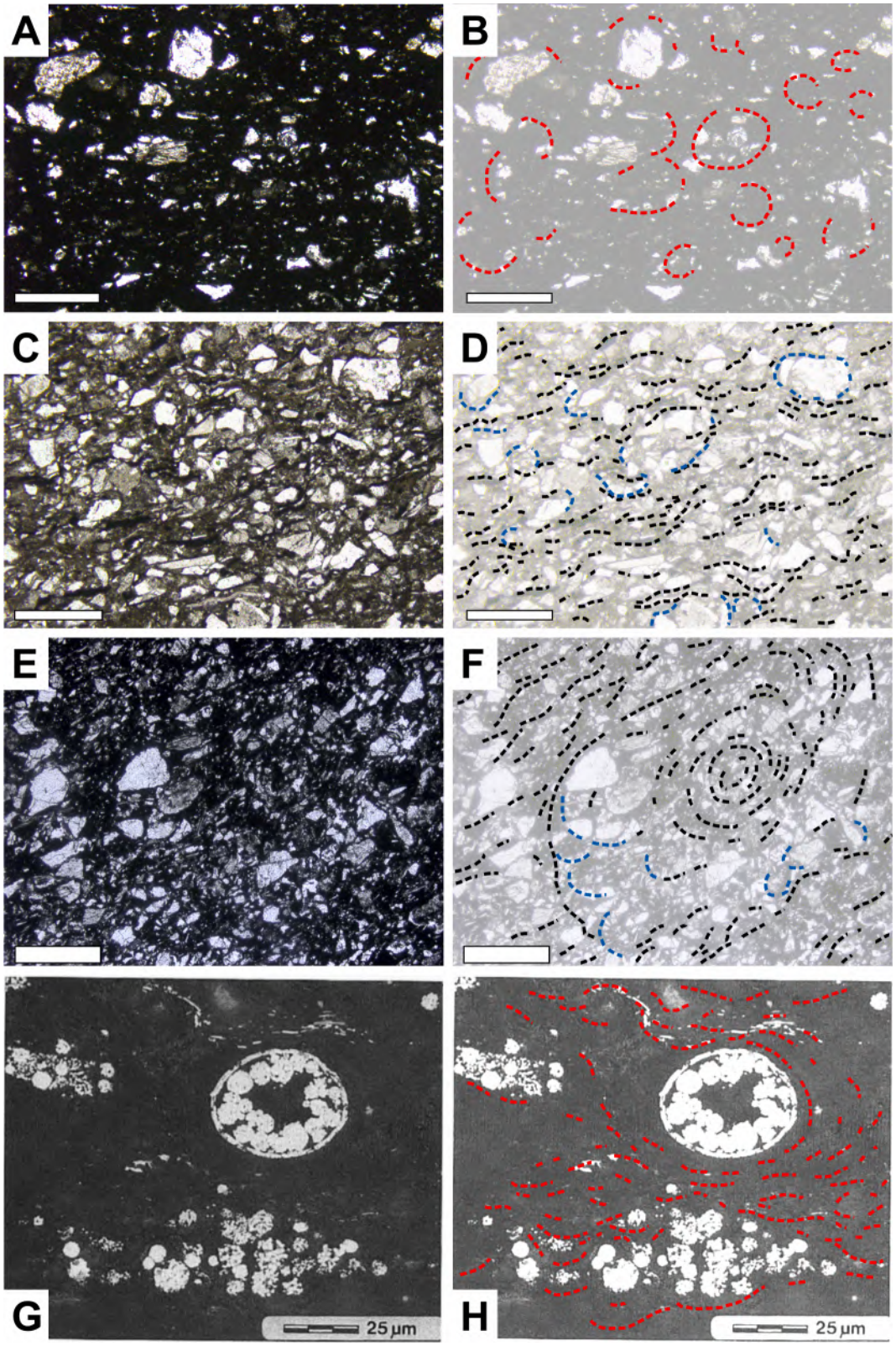


**Fig. 6.** Examples of grain clusters and matrix fabrics observed in the RAB-FD00019 core and respective graphic interpretations. (A, B) Transmitted light photomicrograph displaying abundant organic-rich matrix with circular and semi-circular grain alignments delimiting rounded clusters of clasts at 130 m depth. (C, D) Crinkled and anastomosed matrix fabrics (black dashed lines) around amalgamated irregular and circular grain clusters (blue dashed lines) at 125 m depth. (E, F) Incipient concentric cluster apparently amalgamated with other circular clusters as defined by silt and sand grain alignments (blue dashed lines) and matrix fabric (black dashed lines) at 134 m depth. (G, H) VSM test within organic-rich fine-grained deposits at Jacadigo hill illustrated by Urban et al. (1992). Note "framboidal pyrite" (Urban et al., 1992) in matrix and inside the test, the anastomosed matrix fabric, clay mineral coating on the test and aligned silt grains (red dashed lines). Scale bars: 500 µm (except for G and H). (For interpretation of the references to color in this figure legend, the reader is referred to the web version of this article.)

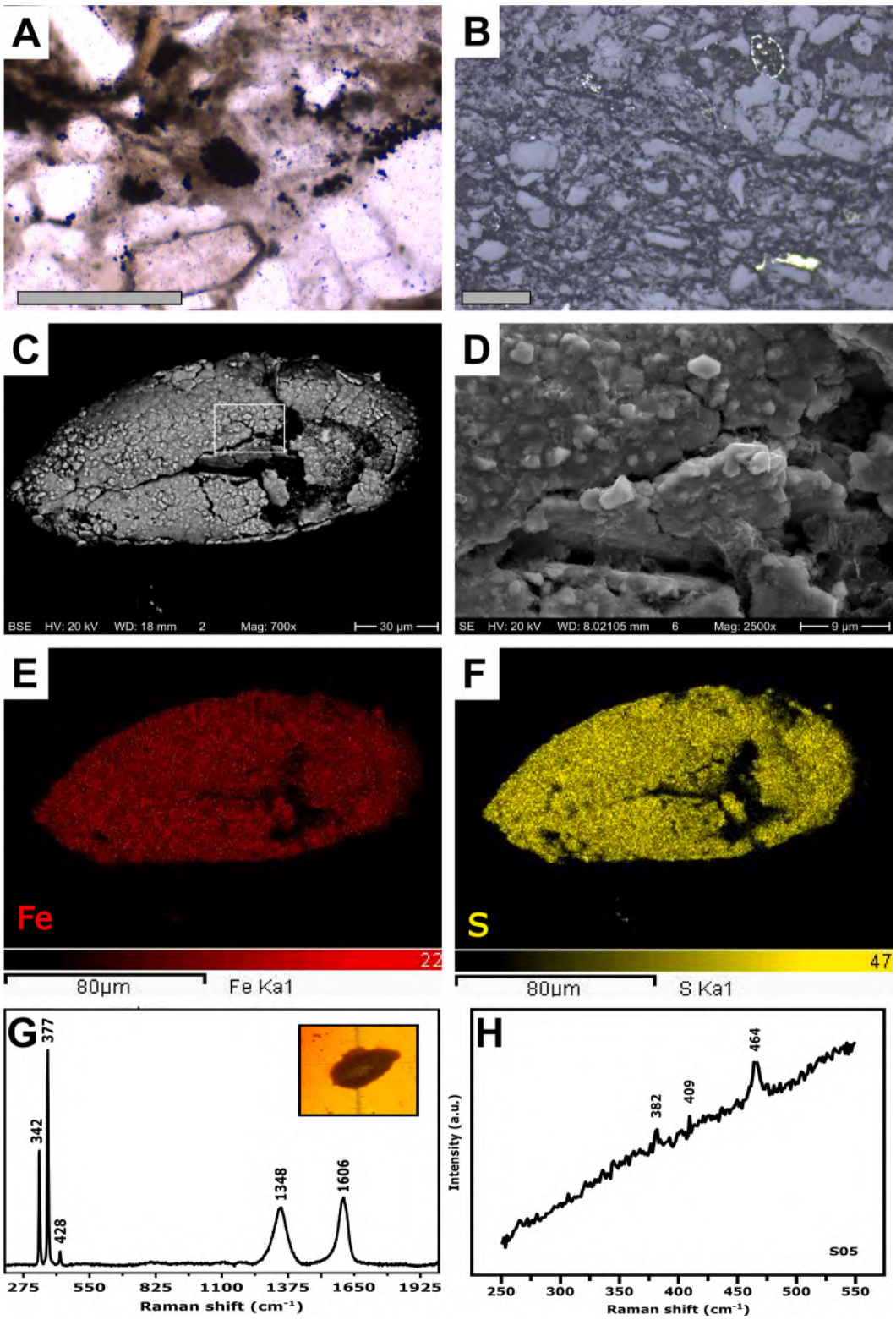


**Fig. 7.** Test preservation in the RAB-FD00019 core. (A) Fine-grained pyrite internal mold of VSM test at 115 m depth. (B) Reflected light photomicrograph highlighting bright yellowish fine-grained pyrite crystals dispersed in the matrix and as coarse-grained amalgamated euhedral crystals and fine-grained crystals around and within VSM tests at 104 m depth. (C) SEM backscattered image of an isolated specimen of *Bonniea dacruchares* Porter, Meisterfeld and Knoll 2003 found at 125 m depth. (D) SEM secondary electron image detailing the test surface in white square in C. (E) EDS map of iron (Fe) concentration in red. (F) EDS map of sulfur (S) concentration in yellow. (G) Montage of different Raman spectra of an isolated test recovered by acid maceration, showing close association of kerogen (peaks centered at 1348 relative $cm^{-1}$ and 1606 relative $cm^{-1}$) and pyrite (peaks centered at 342 relative $cm^{-1}$ and 428 relative $cm^{-1}$). (H) Raman spectra showing quartz O-Si-O molecules vibration bands centered at ca. 464 $cm^{-1}$. Grey scale bar: 200 µm. (For interpretation of the references to color in this figure legend, the reader is referred to the web version of this article.)

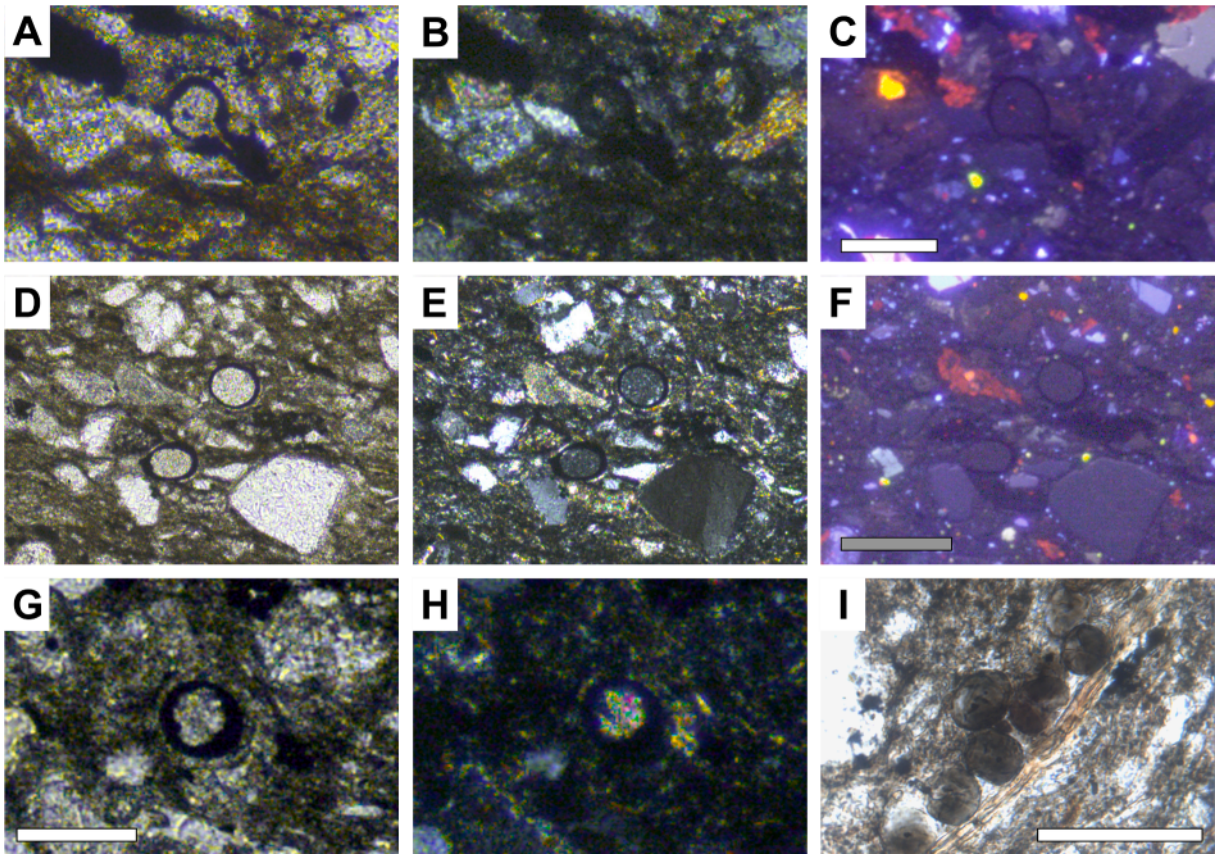


**Fig. 8.** Petrographic features of microfossils in the RAB-FD00019 core. (A-C) Transmitted light (A), crossed Nicols (B), and cathodoluminescence (C) images of a VSM filled by matrix at 134 m depth. Note similarity in composition inside and outside the test as well as the very fine quartz and carbonate silt grains represented by points of purple and red luminescence, respectively. (D-F) Transmitted light (D), crossed Nicols (E) and cathodoluminescence (F) images of two VSMs filled by quartz cement at 115 m depth. Note homogeneity of fine-grained quartz and clay mineral coatings on grains. (G, H) Transmitted light (G) and crossed Nicols (H) images of a VSM filled by carbonate at 104 m depth. Note high birefringence and faceted crystal habit of the test fill. (I) Sphaeromorphic acritarchs aligned along a detrital mica flake within matrix at 115 m depth. White scale bar: 100 μm. Grey scale bar: 200 μm. (For interpretation of the references to color in this figure legend, the reader is referred to the web version of this article.)

Density Estimate (KDE) plot (Fig. 11C), one between 1800 and 2000 Ma, and the other between 700 and 800 Ma, at 737 Ma (Fig. 11D, F), with a weighted mean age of 749 ± 3 Ma (MSWD = 1.51) (Fig. 11E). The weighted mean age of the younger population was calculated using 18 zircon dates with a continuous spread from 719 ± 15 Ma to 773 ± 17 Ma (Fig. 11B). Six younger dates, including two of Cryogenian age, are distributed between 719 ± 15 Ma and 690 ± 18 Ma (Fig. 11B; Table S5).

Thermal overprinting of these zircon grains due to Brasiliano-Pan Africano events is unlikely. The Jacadigo Group is characterized by sub-green schist facies paragenesis (D'el Rey, 2016), consistent with estimated maximum temperatures during diagenesis and anchimetamorphism of 170 to 260 °C (Angerer et al. 2021), with preservation of organic-walled microfossils and with the mean temperature of 279 °C calculated here for organic maturation of kerogen based on Raman spectra (SOM 1, 2).

Thus, our correlation of the VSM-bearing, organic-rich, fine-grained deposits of the Urucum Formation at Jacadigo and Rabicho hills allow us to establish a conservative maximum depositional age for both studied succession and the VSM assemblage at 749 ± 3 Ma. The Cryogenian age dates found within a glacially influenced succession at Jacadigo hill and previously reported Cryogenian detrital zircon grains in the overlying glaciogenic Santa Cruz Formation (Frei et al., 2017) point to a Late Tonian to Early Cryogenian source of detrital zircon for both units of the Jacadigo Group.

Our geochronological results narrow the age constraints on the deposition of the studied successions to sometime between the conservative weighted mean age of 749 ± 3 Ma (Tonian) and the available minimum age of 587 ± 7 Ma (Ediacaran) for anchimetamorphism (Piacentini et al., 2013). These results alone do not rule out a Tonian age for the studied deposits and microfossils, which would be in keeping with the present consensus of the temporal distribution of VSMs.

However, the dominance of glacial microfacies in the studied material is highly suggestive of a younger, Cryogenian age. Even considering the interval defined by the Paleoproterozoic age of the basement and the Ediacaran age of anchimetamorphism, only two glacial episodes are known – the Sturtian and Marinoan global glaciations, both within the Cryogenian Period (e.g. Hoffman et al., 2017; Freitas et al., 2021).

Moreover, the presence of Early Cryogenian zircon grains in our material provides additional support for the interpretation of a Cryogenian age for the rocks and in situ microfossils studied here. Indeed, elsewhere Freitas et al. (2021) have more specifically correlated the Jacadigo Group with Neoproterozoic cryochrons and have proposed a Marinoan age for the organic-rich fine-grained successions at Jacadigo and Rabicho hills.

### 4.5. *Systematic paleontology*

The newly discovered VSMs in organic-rich fine-grained deposits of the upper Urucum Formation at Rabicho hill comprise cup- to tear-shaped tests, circular in transverse section, that may taper toward a single opening, rimmed or not by a distinct collar, while at the opposite end the aboral pole may be rounded or slightly pointed. The tests vary widely in size from 30 to 200 μm long and 30 to 140 μm wide and present greater morphological diversity than the VSMs previously

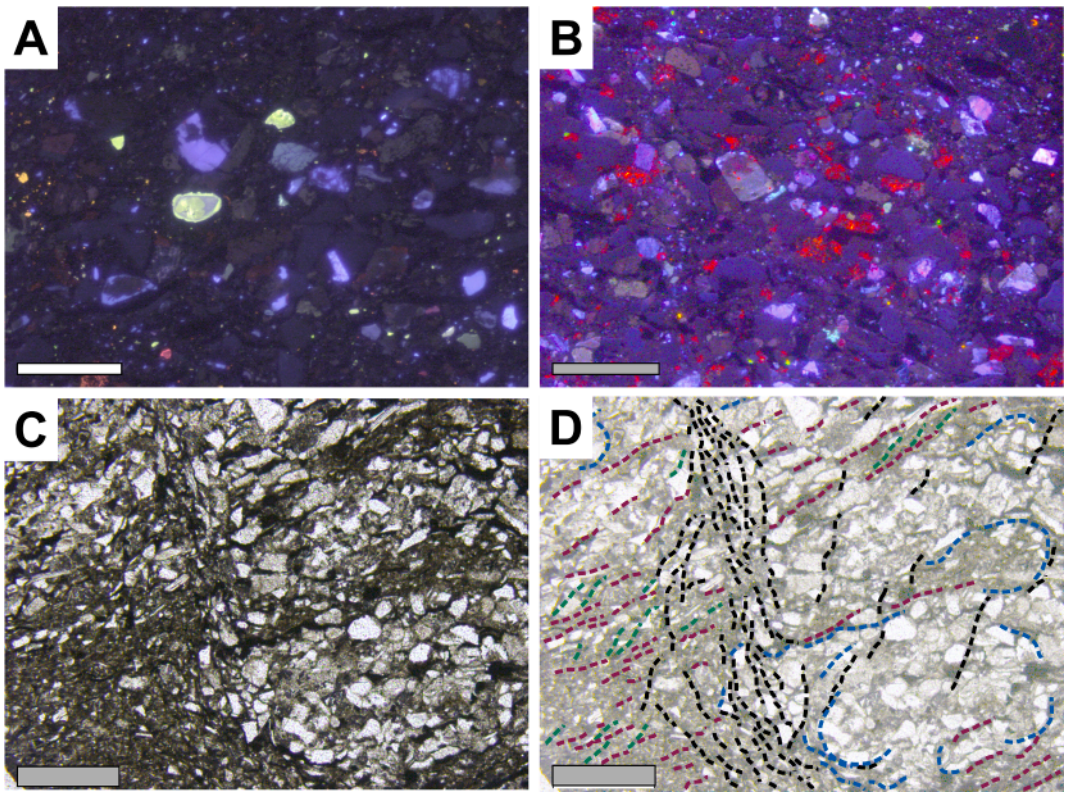


**Fig. 9.** Cement and *syn*-sedimentary fault domains in the RAB-FD00019 core. (A) Cathodoluminescence image showing plagioclase (green luminescence) and quartz (bright purple luminescence) overgrowth at 120 m depth. (B) Cathodoluminescence image highlighting preferential calcite replacement (red luminescence) of silt and sand grains around sub-circular grain clusters at 104 m depth. (C, D). Transmitted light photomicrograph and graphic interpretation of syn-sedimentary fault domain (black dashed lines) affecting grain clusters (blue dashed lines) and two sets of matrix fabrics (red and green dashed lines) at 125 m depth. White scale bar: 200 μm. Grey scale bar: 500 μm. (For interpretation of the references to color in this figure legend, the reader is referred to the web version of this article.)

reported in dolostone clasts near the base of the formation (Morais et al., 2019; Table 1). Of the approximately 100 specimens of VSMs available in thin sections for the present study, 47 exhibited longitudinal sections parallel to the thin section surface suitable for detailed examination of critical features and assignment to seven species: *Cycliocyrillium simplex*, *Bonniea dacruchares*, *B. pytinaia*, *Palaeoarcella athanata*, and *Trigonocyrillium horodyskii*, originally described by Porter et al. (2003); and *Limeta lageniformis* and cf. *Taruma rata*, originally described by Morais et al. (2017). *Pakupaku kabin,* described by Riedman et al. (2018), *Palaeoarcella athanata*, *B. pytinaia*, and *Bombycion micron* are here reported for the first time in the Urucum Formation (Table 1).

Domain Eucarya Woese et al., 1990
Vase-shaped Microfossils
Genus *Cycliocyrillium* Porter et al., 2003 emend. Morais et al., 2017
Type species: *Cycliocyrillium simplex* Porter et al., 2003.
Other species: *Cycliocyrillium torquata* Porter et al., 2003.
Emended diagnosis: Bulbous to pyriform VSMs having a circular aperture either flush with the test or associated with a narrow collar or short, uncurved neck, not exceeding one-tenth the total length of the specimen; angle between the apertural plane and the aboral axis ~90°.

*Cycliocyrillium simplex* Porter et al., 2003
Fig. 12A; Table 1

1933 Fossil II Ewetz (1933), p. 509, fig. 6.
1979 "Enigmatic, 'bag-shaped', 'chitinozoan-like' microfossils" Vidal,
p. 24, plate 6, figs. A; B.
1980 "Vase-shaped microfossils" Knoll and Vidal, p. 208, fig. 1D–G.
1980 "Flask-shaped forms" Binda and Bokhari, p. 71, fig. 1D–E.
1983 "Vase-shaped microfossils" Knoll and Calder, p. 489, plate 61, fig 2; 3; 7; 8.
1989 *Melanocyrillium* Knoll *et al.*, p. 138, fig. 7.9.
2003 Cycliocyrillium simplex Porter *et al.*, p. 415, fig. 6.1–6.9.
2010? *Melanocyrillium* cf. *Melanocyrillium hexodiadema* Sergeev and Schopf, p. 386, fig. 14.3.
2017 *Cycliocyrillium simplex* Cohen, Irvine and Strauss, p. 15, figs. 4A–C; 7B-C.
2017 *Cycliocyrillium simplex* Morais *et al.*, p. 5, figs. 2.1–2.5.
2018 *Cycliocyrillium simplex* Riedman *et al.*, figs.3.7, 3.11, 4.12, 4.13, 5.7–5.9, 5.11, 5.13
Holotype: HUPC# 64455, upper Tonian (~742 ± 6 Ma), Kwagunt Formation, Chuar Group, Grand Canyon, Arizona (Porter et al., 2003; p. 415, fig. 6.1–6.9).
Materials: N = 4. Thin sections GP/5E-4374 and GP/5E-4375 from levels 115.4 m and 125.1 m, respectively, below top of core RAB-FD00019 (Fig. 2), Urucum Formation, Jacadigo Group (Corumbá, Brazil).
Diagnosis: Specimens of *Cycliocyrillium* whose apertural margin is not thickened or set off from the rest of the test by a short neck. Smooth apertural margin, flush with the rest of the test.
Description: Specimens with bulbous tests and circular aperture, without a collar or neck. Test lengths range from 134 μm to 181 μm (x = 149 μm, σ = 22 μm), test widths range from 77 μm to 119 μm (x = 92 μm, σ = 18 μm) and length–width ratios range from 1.21 to 2.35 (x = 1.67, σ = 0.48). Aperture not measurable in practically all specimens.
Remarks: Specimens are bigger than those found in dolostone clasts within the Urucum Formation (Morais et al., 2017; Morais et al., 2019): test lengths are 134 to 181 μm *vs.* 50 to 139 μm and widths are

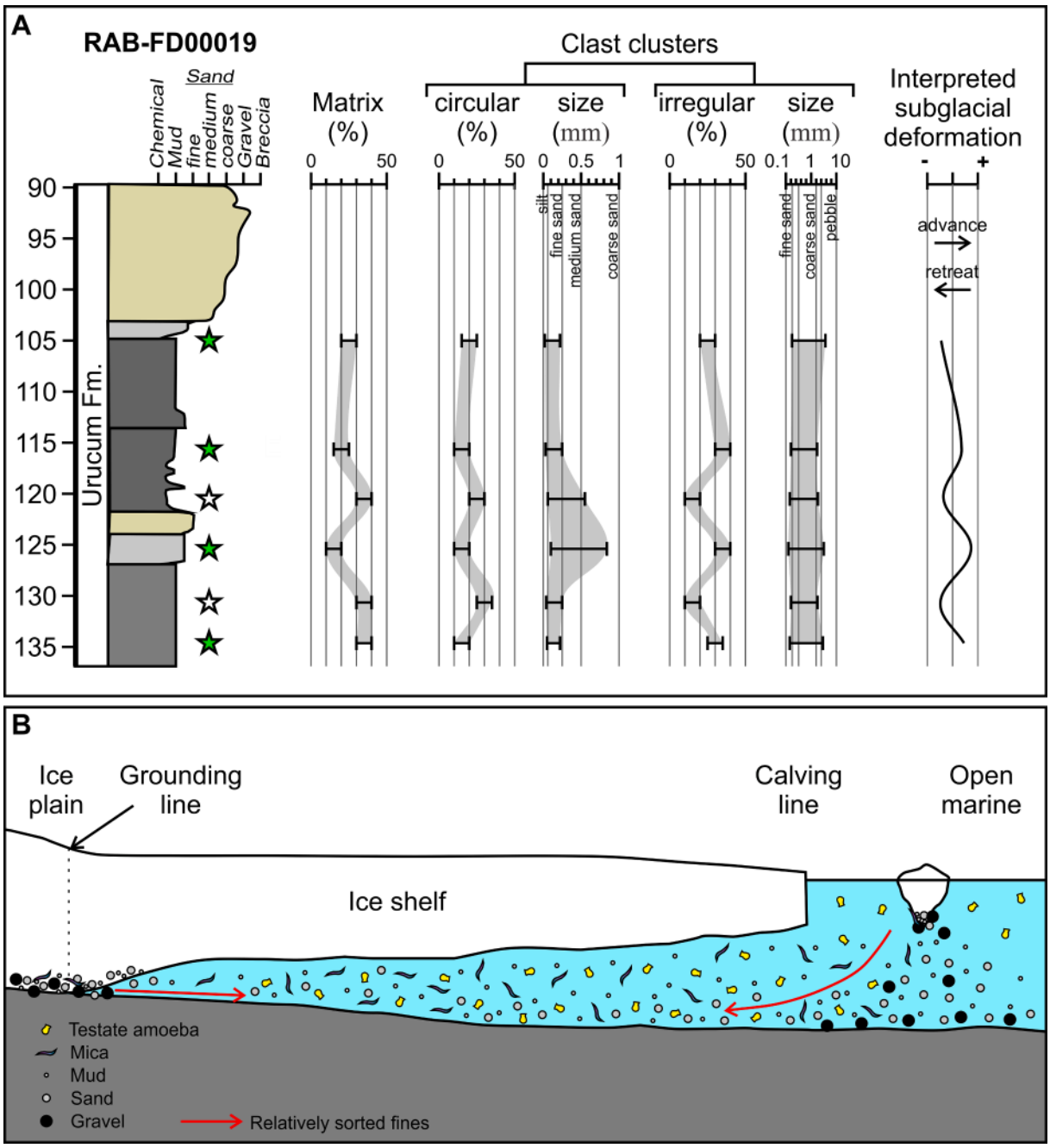


**Fig. 10.** Sedimentary setting for the VSM-bearing, organic-rich, fine-grained succession of the Urucum Formation. (A) Variation of the abundance of matrix and clast clusters and its interpreted meaning along the studied succession in the RAB-FD00019 core. (B) Reconstruction of sedimentary setting beneath an ice shelf between ice grounding and calving lines for the in situ entombment of the VSM assemblage described here (modified from Domack et al., 1999).

77 to 119 μm *vs.* 42 to 96 μm. Additionally, the VSMs are also bigger if compared to Kwagunt Formation (L = 40–110 μm; W = 35–75 μm); Callison Lake Formation (L = 59–164 μm; W = 40–102 μm); Eleonore Bay Group (L = 34–126 μm; W = 23–65 μm); and Visingsö Group (L = 41–67 μm; W = 18–34 μm) (Porter et al., 2003; Morais et al., 2017, supp. material; Riedman et al., 2018).

Genus *Limeta* Morais et al., 2017

Type species: *Limeta lageniformis* Morais et al., 2017

*Limeta lageniformis* Morais et al., 2017

Fig. 12B; Table 1

2017 *Limeta lageniformis* Morais *et al.*, p. 400, figs. 4.4; 6.7–6.9; 7.5; 7.6.

2019 *Limeta lageniformis* Morais *et al.*, p. 5, figs. 2.9–13.

Holotype: GP/5T: 2529 F from the Neoproterozoic Urucum Formation, Jacadigo Group, Corumbá, Brazil (Morais *et al.*, p. 400, figs. 4.4; 6.7–6.9; 7.5; 7.6).

Diagnosis: VSMs tests having a pyriform to sub-globose body and a long neck, 20–50% the total length of the test, with a simple terminal aperture.

Materials: N = 2. Thin sections GP/5E-4374 and GP/5E-4375 of the 115.4 m at 125.1 m levels, respectively, measured from the top downwards of core RAB-FD00019 (Fig. 2), Urucum Formation, Jacadigo Group (Corumbá, Brazil).

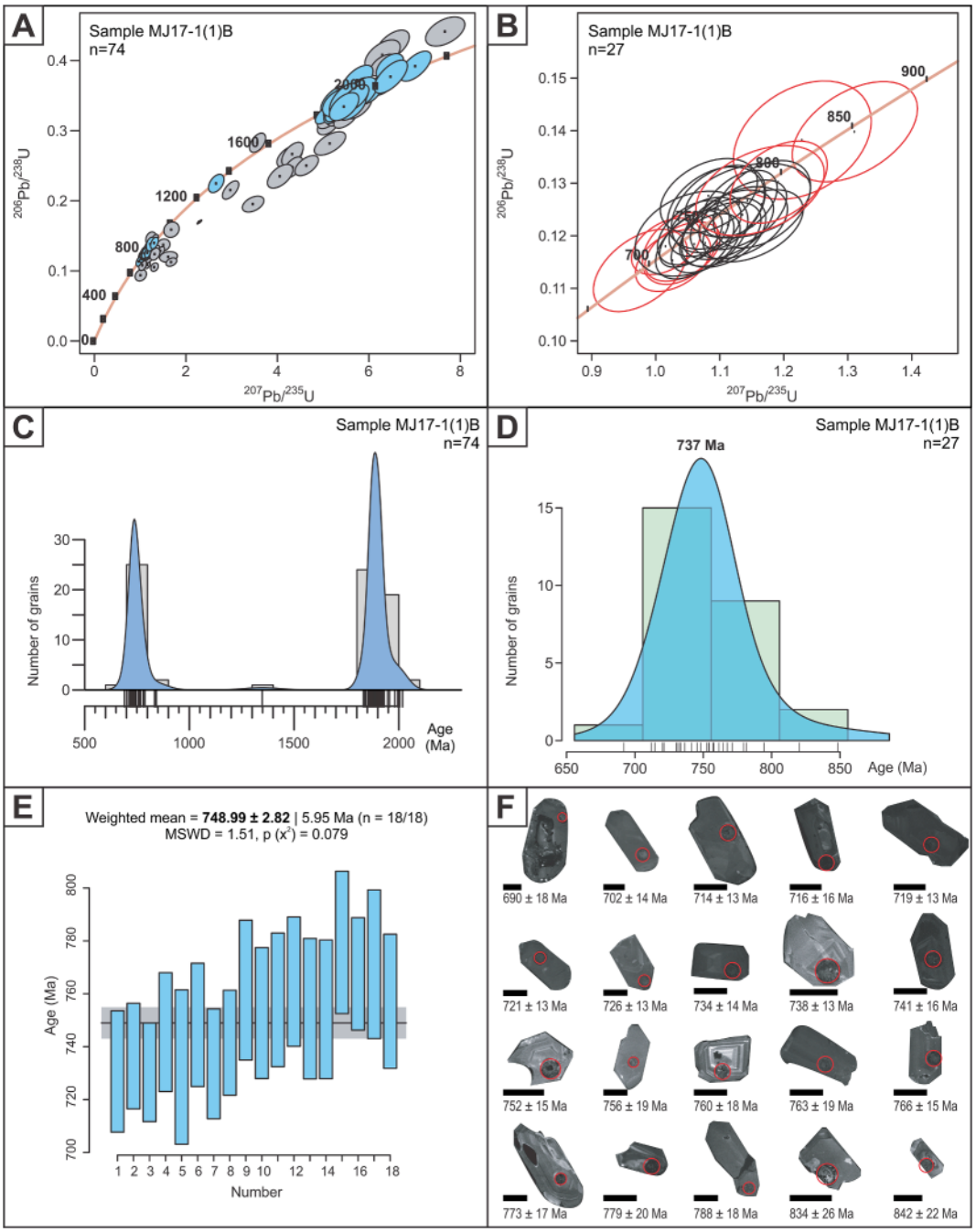


**Fig. 11.** Results of detrital zircon geochronology. (A) Concordia plot of all detrital zircon dates obtained from sample MJ17-1(1)B, representative of the fine-grained, organic rich, VSM-bearing succession of the Urucum Formation at Jacadigo hill. (B) Concordia plot for the younger population found in sample MJ17-1(1)B. Dates excluded from the calculation of the weighted mean age (E) are represented by red ellipses. (C) Kernel Density Estimate (KDE) plot for all detrital zircon dates obtained from sample MJ17-1(1)B. (D) KDE plot for the younger population. (E) Weighted mean age of the younger population. (F) Cathodoluminescence image of examples of dated zircon grains of the younger population. Plots generated with IsoplotR (Vermeesch, 2018). Black scale bars: 50 μm. (For interpretation of the references to color in this figure legend, the reader is referred to the web version of this article.)

Description: Test lengths range from 137 μm to 213 μm, widths from 76 μm to 82 μm, length–width ratios of (x = 1.80, 2.59); neck lengths range from 50 μm to 85 μm, and neck length-total length ratios from 0.26 to 0.40. Aperture is not measurable in practically all specimens.
Remarks: Specimens are bigger than those found in dolostone clasts within the Urucum Formation (Morais et al., 2017; Morais et al.,2019): test lengths are 137 to 213 μm *vs.* 100 to 133 μm and widths are 76 to 82 μm *vs.* 53 to 70 μm. Additionally, the VSMs are also bigger if compared to Kwagunt Formation (L = 67–169 μm; W = 29–62 μm) and Callison Lake Formation (L = 85–198 μm; W = 29–85 μm) (Porter et al., 2003; Morais et al., 2017).

Genus *Bonniea* Porter et al., 2003

Type species: *Bonniea dacruchares* Porter et al., 2003
Other species: *Bonniea pytinaia* Porter et al., 2003
*Bonniea dacruchares* Porter et al., 2003
Fig. 12C; Table 1
1988 *Melanocyrillium* Green *et al.*, p. 839, fig. 4.4.

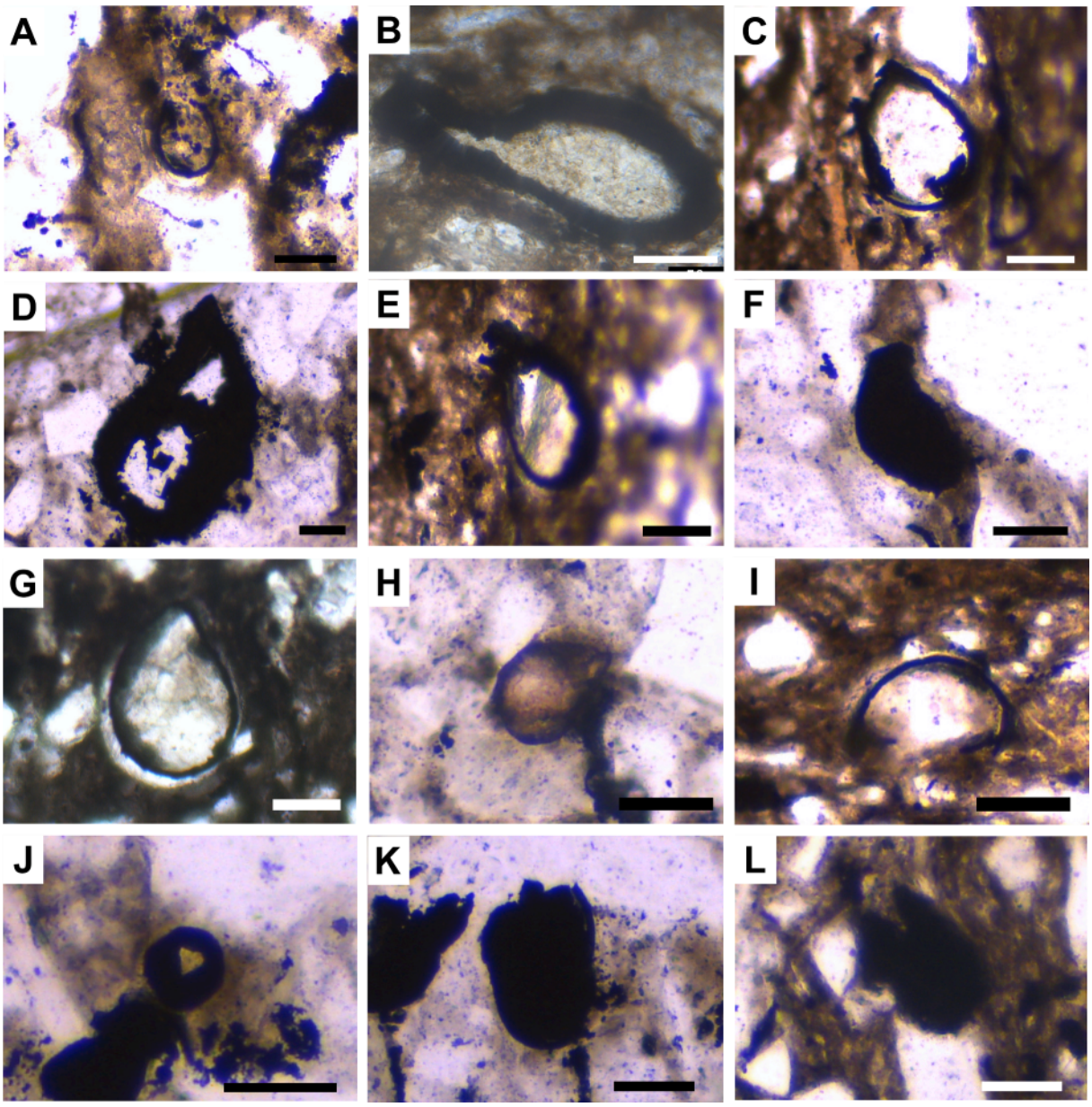


**Fig. 12.** Photomicrographs of representative VSMs from drill core RAB-FD0009 in the Neoproterozoic Urucum Formation, Jacadigo Group, Brazil. Tests in A-G, I-K, have been fully pyritized. (A) *Cycliocyrillium simplex* (GP/5E 4374). (B) Deformed test of *Limeta lageniformis* (GP/5E 4374). (C) *Bonniea dacruchares* (GP/5E 4374). (D-E) *Bonniea pytinaia* (GP/5E 4374). (F) cf. *Bonniea pytinaia* (GP/5E 4374). (G) *Bombycion micron* (GP/5E 4374). (H) Partially pyritized carbonaceous test of *Bombycion micron* (GP/5E 4375). (I) *Palaeoarcella athanata* (GP/5E 4374). (J) Apertural view of pyritized test of *Trigonocyrillium horodyskii* (GP/5E 4374) (K) cf. *Taruma rata* (GP/5E 4374). (L) *Pakupaku kabin* (GP/5E 4374). Scale bars: 50 μm.

1996 "Vase-shaped microfossil (Melanocyrillium sp)", Knoll (1996), pl. 3, fig. 12.
2001 "Curved specimen" Martí Mus, p. 5, Fig. 3I.
2003 *Bonniea dacruchares* Porter *et al.*, p. 417, fig. 9.1–9.15.
2014 *Bonniea dacruchares* Strauss *et al.*, p. 660, fig. 2E.
2017 *Bonniea dacruchares* Cohen, Irvine and Strauss, p. 13, fig. 3A-B.
2017 *Bonniea dacruchares* Morais et al., 2017, p. 6, figs. 3.10–3.11.
2018 *Bonniea dacruchares* Riedman et al., 2018, pgs. 23, 25, 27, figs. 3.12; 4.3; 4.5; 4.9.

Holotype: HUPC# 64,409 from sample AK10-53-13A, Nankoweap Butte locality, Walcott Member, Chuar Group, Grand Canyon, Arizona (Porter *et al.*, p. 417, fig. 9.1–9.15).

Materials: N = 21. Thin sections GP/5E-4373, GP/5E-4374, and GP/5E-4375 of the 104.9 m, 115.4 m, and 125.1 m levels, respectively, measured from the top downwards of core RAB-FD00019 (Fig. 2), Urucum Formation, Jacadigo Group (Corumbá, Brazil).

Diagnosis: Specimens of the genus *Bonniea* with tests having length-to-width ratios of less than two and concavity greater than 30°. Aperture may be slightly thickened (Porter et al., 2003).

Description: Tests range from 49 μm to 159 μm in length (x = 115 μm, σ = 25 μm), from 29 μm to 106 μm in width (x = 71 μm, σ = 19 μm), and from 1.28 to 2.11 in length–width ratio (x = 1.65, σ = 0.20). Aperture is not measurable in practically all specimens.

Remarks: Specimens are bigger than those found in dolostone clasts within the Urucum Formation (Morais et al., 2017; Morais et al., 2019): test lengths are 49 to 144 μm *vs.* 65 to 88 μm and widths are 29 to 106 μm *vs.* 46 to 65 μm. Additionally, the VSMs are similar if compared to Kwagunt Formation (L = 65–180 μm; W = 35–90 μm); Callison Lake Formation (L = 60–153 μm; W = 35–90 μm) and Black

River Dolomite (L = 67–125 μm; W = 41–77 μm) (Porter et al., 2003; Morais et al., 2019; Riedman et al., 2018).

*Bonniea pytinaia* Porter e al., 2003
Fig. 12D-F; Table 1

2003 *Bonniea pytinaia* Porter *et al.*, p. 418, figs. 9.16–9.23; 18.2.
2017 *Bonniea pytinaia* Cohen, Irvine and Strauss, p. 14, fig. 3C–E, J.
2018 *Bonniea pytinaia* Riedman *et al.*, pgs. 22; 25; 27, figs. 3.9–3.10; 4.4; 4.6–4.8; 5.5–5.6; 5.10.
Holotype: HUPC# 64,410 from sample AK10-53-13A, Nankoweap Butte locality, Walcott Member, Chuar Group, Grand Canyon, Arizona (Porter *et al.*, p. 418, figs. 9.16–9.23; 18.2).
Materials: N = 5. Thin sections GP/5E-4374 and GP/5E-4375 of the 115.4 m 125.1 m levels, respectively, measured from the top downwards of core RAB-FD00019, (Fig. 2). Urucum Formation, Jacadigo Group (Corumbá, Brazil).
Diagnosis: Specimens of the genus *Bonniea* that have a test with a length-to-width ratio of two or greater and concavity less than 30°.
Description: Tests range from 134 μm to 166 μm in length (x = 144 μm, σ = 13 μm), 62 μm to 103 μm in width (x = 74 μm, σ = 15 μm) and 1.31 to 2.25 in length–width ratios (x = 1.99, σ = 0.34). Aperture is not measurable in practically all specimens. Specimen shown in Fig. 12F is here included in this taxon with reservations, due to poor preservation of the aperture.
Remarks: This species has never been observed within dolostone clasts near the base of the Urucum Formation. VSMs are bigger than those found in Kwagunt Formation (L = 80–160 μm; W = 30–70 μm); Callison Lake Formation (L = 79–181 μm; W = 31–81 μm) and similar to Black River Dolomite (L = 57–184 μm; W = 26–78 μm) (Porter et al., 2003; Riedman et al., 2018).

Genus *Bombycion* Porter et al., 2003

Type species: *Bombycion micron* Porter et al., 2003
*Bombycion micron* Porter et al., 2003
Fig. 12G-H; Table 1
2003 *Bombycion micron* Porter *et al.*, p. 421, figs. 13.1–13.4.
2014 *Bombycion micron* Strauss *et al.* Strauss *et al.*, p. 660, fig. 2D.
2018 *Bombycion micron* Riedman *et al.*, pgs. 22; 25, figs. 3.4; 3.6; ? 4.1–4.2.
Holotype: HUPC# 64,410 from sample AK10-53-13A, Nankoweap Butte locality, Walcott Member, Chuar Group, Grand Canyon, Arizona (Porter *et al.*, p. 423, figs. 13.1–13.4)
Materials: N = 4. Thin sections GP/5E-4374 and GP/5E-4375 of the 115.4 m 125.1 m levels, respectively, measured from the top downwards of core RAB-FD00019, (Fig. 2). Urucum Formation, Jacadigo Group (Corumbá, Brazil).
Diagnosis: Vase-shaped microfossil with apertural plane tilted such that it is flush with the side of the test.
Description: Tests range from 85.7 μm to 195.6 μm in length (x = 151.1 μm, σ = 52.3 μm), 57 μm to 130.4 μm in width (x = 96.9 μm, σ = 35.4 μm) and 1.5 μm to 1.7 μm in length–width ratios (x = 1.6, σ = 1.5). Aperture diameters range from 17 μm to 65.2 μm (x = 40.8 μm, σ = 20.1 μm).
Remarks: This species has never been observed within dolostone clasts near the base of the Urucum Formation. VSMs are bigger than those found in the Kwagunt Formation (L = 60–195 μm; W = 39–85 μm) and similar to the Black River Dolomite (L = 59–155 μm; W = 26–78 μm) (Porter et al., 2003; Riedman et al., 2018). Aperture not measurable in the specimens.

Genus *Palaeoarcella* Porter et al., 2003

Type species. *Palaeoarcella athanata* Porter et al., 2003, by monotypy.

*Palaeoarcella athanata* Porter et al., 2003
Fig. 12I; Table 1
2003 *Palaeoarcella athanata* Porter *et al.*, p. 419, figs. 11.1–11.6.
2014 *Palaeoarcella athanata* Strauss *et al.*, p. 660, fig. 2B.
2017 *Palaeoarcella athanata* Cohen, Irvine and Strauss, p. 17, fig., 5D-F.
2018 *Palaeoarcella athanata* Riedman *et al.*, pgs. 22; 25, figs. 3.5; 3.8; 4.10–4.11.
Holotype: HUPC# 62,988 from sample AK10-53-13F, Nankoweap Butte locality, Walcott Member, Chuar Group, Grand Canyon, Arizona (Porter *et al.,* p. 419, figs. 11.1–11.6).
Materials: N = 4. Thin sections GP/5E-4373 and GP/5E-4375 of the 104.9 m 125.1 m levels, respectively, measured from the top downwards of core RAB-FD00019, (Fig. 2). Urucum Formation, Jacadigo Group (Corumbá, Brazil).
Diagnosis: Hemispherical VSMs with a test length approximately half that of test width. Test rounded, without indentations. Aperture circular, invaginated.
Description: Hemispherical tests with invaginated aperture. Test length ranges from 28 μm to 47 μm (x = 39 μm, σ = 8 μm), test width ranges from 78 μm to 138 μm (x = 99 μm, σ = 27 μm) and length–width ratios range from 0.20 to 0.56 (x = 0.43, σ = 0.17). Only one aperture diameter (90 μm) was measurable.
Remarks: This species has never been observed within dolostone clasts near the base of the Urucum Formation. VSMs are bigger than those found in Kwagunt Formation (L = 20–40 μm; W = 40–70 μm) and Black River Dolomite (L = 28–29 μm; W = 46–58 μm) (Porter et al., 2003; Riedman et al., 2018).

Genus *Trigonocyrillium* Porter et al., 2003

Type species: *Trigonocyrillium horodyskii* (Bloeser, 1985) Porter et al., 2003
Other species: *Trigonocyrillium fimbriatum* (Bloeser, 1985) Porter et al., 2003
Diagnosis: Pyriform to bulbous VSMs with an equilateral triangular aperture.
*Trigonocyrillium horodyskii* (Bloeser, 1985) Porter et al., 2003
Fig. 12J; Table 1
2003 *Trigonocyrillium horodyskii* (Bloeser, 1985) Porter *et al.*, p. 412, fig. 5.1–5.19.
Holotype: University of California at Los Angeles (UCLA) catalogue number 58,975 from Walcott Member, Kwagunt Formation, Chuar Group, Grand Canyon, Arizona (Porter *et al.*, p. 412, fig. 5.1–5.19).
Materials: N = 1. Thin section GP/5E-4374 of the 115.4 m level measured from the top downwards of core RAB-FD00019 (Fig. 2), Urucum Formation, Jacadigo Group (Corumbá, Brazil).
Diagnosis: Specimens of the genus *Trigonocyrillium* with unadorned apertural margins.
Description: The specimen, viewed in cross section, exhibits the diagnostic equilateral triangular aperture with subrounded apices; sizes equal to 20 μm. Other morphometric parameters were not measurable.
Remarks: Only the aperture of one specimen was observed, but it fits in diagnosis for the species (Porter et al., 2003).

Genus *Taruma* Morais et al., 2017

Type species: *Taruma rata* Morais et al., 2017
cf *Taruma rata* Morais et al., 2017
Fig. 12K; Table 1
2017 Taruma rata Morais et al., 2017, pg. 394, fig. 1.4; pg. 397; fig. 4.4; pg.399; figs. 5.7–5.9.
Holotype: Holotype GP/5T 2533 B from the Neoproterozoic Urucum Formation, Jacadigo Group, Corumbá, Brazil (Morais et al., 2017, pg. 394, fig. 1.4; pg. 397; fig. 4.4; pg.399; figs. 5.7–5.9).

Material: N = 1. Thin section GP/5E-4374 of the 115.4 m level measured from the top downwards of core RAB-FD00019 (Fig. 2), Urucum Formation, Jacadigo Group (Corumbá, Brazil).
Diagnosis: VSMs with nearly cylindrical test having a rounded aboral end and a flat to low roof-like oral surface with a narrow central circular aperture.
Description: Specimen shows diagnostic features as cylindrical test with a rounded aboral end and a flat roof-like oral surface, measuring 85 μm in length and 53 μm in width. The surface is totally pyritized and the aperture is not clear.
Remarks: Pyritization impedes visualization of the double wall evident in specimens described by Morais et al. (2017) as well as wall structure and details of the aperture. What suggests its identification as *Taruma rata* is its cylindrical shape and rounded aboral pole, a shape unique to this species among formally named VSM species. Until other, better preserved specimens can be found to confirm this identification, we shall refer to this specimen as cf. *Taruma rata*.

Genus *Pakupaku* Riedman et al., 2018

Type species: *Pakupaku kabin* Riedman et al., 2018
cf. *Pakupaku* Riedman et al., 2018
Fig. 12L; Table 1
2018 *Pakupaku kabin* Riedman et al., 2018, pg. 11, fig. 6.1–6.2.
Holotype: Holotype.—(Fig. 6.1, 6.2), Accession number CPC43685, slide Tas 10–41(par), England Graticule coordinates F69-0, from Bertha Road locality, lower Black River Dolomite, Togari Group, Tasmania. (Riedman et al., 2018, pg. 11, figs. 6.1–6.2).
Material: N = 2. Thin section GP/5E-4374 of the 115.4 m level and GP/5E-4375 of the 125.1 m level measured from the top downwards of core RAB-FD00019 (Fig. 2), Urucum Formation, Jacadigo Group (Corumbá, Brazil).
Diagnosis: Vase-shaped microfossil with pyriform test and aperture (when viewed oral end-on) with shape of biconvex lens or an ellipse with two pointed ends. As viewed in profile, the aperture has a gaping appearance like a wedge has been removed.
Description: Specimen shows diagnostic features as a pyriform test and aperture (when viewed oral end-on) with shape of biconvex lens or an ellipse with two pointed ends, measuring 150 and 155,5 μm in length and 61 and 87,5 μm in width. Aperture measuring 25 and 27.7 μm.
Remarks: The profile view in the thin section allowed to see the gaping appearance in *Pakupaku kabin*, like a wedge has been removed, as described by Riedman et al. (2018).

## 5. Significance of this discovery

The discovery of VSMs preserved within the fine-grained succession in the upper Urucum Formation impacts significantly upon current thinking on several aspects of late Neoproterozoic Earth history. Most importantly, it shows that specific VSM taxa (*Cycliocyrillium simplex, Limeta lageniformis, Bonniea dacruchares, Bonniea pytinaia, Bombycion micron, Palaeoarcella athanata, Trigonocyrillium horodyskii* and *Pakupaku kabin*), usually thought to be restricted to the Tonian, persisted into the Cryogenian record. Although our geochronologic results do not exclude a Tonian age for the microfossils, facies analysis strongly points to deposition in a proximal glacially influenced, hence Cryogenian setting. This unusual facies containing the VSMs, now becomes a promising new target for micropaleontological investigation in Cryogenian successions worldwide.

All four levels containing VSMs in drill core RAB-FD00019 (at depths of 134.5, 125.1 m, 115.4 m and 104.9 m) present similar petrographic evidence characteristic of glacial deformation but also similar species composition and diversity of scattered three-dimensional, pyrite-encrusted and permineralized complete tests, and associated abundant kerogen. Except for species composition and diversity, these characteristics contrast with what Morais et al. (2017) and Morais et al. (2019) observed in the VSM-bearing dolostone clasts in diamictites from the same formation. Nine taxa of VSMs are now known from the siliciclastic deposits studied here and seven from the carbonate clasts, five of which are common to both: *Cycliocyrillium simplex*, *Bonniea dacruchares*, and *Trigonocyrillium horodyskii*, *Limeta lageniformis* and cf. *Taruma rata* (Porter et al., 2003; Morais et al., 2017). *Bonniea pytinaia*, *Bombycion micron*, *Palaeoarcella athanata and Pakupaku kabin* have been observed only in the organic-rich fine-grained facies of the Urucum Formation, whereas *Cycliocyrillium torquata* Porter et al. (2003) and *Palaeoamphora urucumense* Morais et al. (2017) are only known in the carbonate clasts.

Presuming that the microfossiliferous dolostone clasts come from a source within the Urucum Formation itself, as proposed by Freitas et al. (2021), the total number of species in the carbonate clast and organic-rich fine-grained facies assemblages now comes to 12. The Callison Lake and Kwagunt assemblages, with 13 and 16 species, respectively, show the greatest diversity among VSMs assemblages (Porter et al., 2003; Cohen et al., 2017; Riedman et al, 2018; Morais et al., 2019). We predict that reexamination of other VSM occurrences worldwide will similarly reveal greater morphological diversity than previously acknowledged.

Except for *Taruma rata*, all Urucum taxa are also known in Tonian assemblages. Four of the taxa – *C. simplex*, *C. torquata*, *Bonniea dacruchares*, and *B. pytinaia*, are part of Riedman et al.'s (2018) *Cyclocyrillium simplex* assemblage, proposed as biostratigraphically useful for identifying upper Tonian rocks. Given the evidence presented here that these taxa extended into the Cryogenian, this concept is here called into question. Nevertheless, it should be noted that the fifth taxon of Riedman *et al.*'s assemblage, *Melanocyrillium hexadiadema*, continues to be restricted to Tonian strata.

The new assemblage from the Urucum Formation indicates that despite the apparent decline of the record of marine testate protistans (VSMs) near the end of the Tonian period, several Tonian VSM taxa persisted into the Cryogenian, specifically into the Marinoan cryochron (Freitas et al., 2021). The VSMs occur in situ in the organic-rich fine-grained facies, that is, they are undoubtedly the same age as these deposits. But whether they represent benthic autochthonous elements or parautochthonous components derived from the water column beneath or adjacent to an ice shelf or from cryoconite holes or pans on the ice surface remains to be determined.

Another open question remains regarding their relationship to continental arcellinids, with which they are most often compared. Are they merely morphological analogues or could they be homologous with modern lineages? Possibly, the extreme stresses in the marine environment at the end of the Tonian and the onset of intense Cryogenian glaciation may have favored their transition to freshwater habitats and, later, to continental settings, via, for example, adaptation to meltwater-derived, oxygen-rich freshwater lenses overlying denser seawater in restricted marine environments, such as fjords, during glaciation (Hoffman et al., 2017; Lechte et al., 2019). The discovery of arcellinid-like microfossils in marginal depositional settings and their reduction in marine environments during the Cryogenian and Ediacaran is predicted by this model and might represent the first step to establish the timing of continental conquest by testate amoebae.

## 6. Conclusions

Pyritized tests exhibiting morphologies consistent with those of both modern arcellinid testate amoebae and Tonian vase-shaped microfossils (VSMs) have been found in situ in deposits of the Urucum Formation displaying varied evidence of glacial influence correlated with the Marinoan global glaciation. The maximum age of deposition of these shales and microfossils, as determined from detrital zircon, is conservatively established at 749 ± 3 Ma, late Tonian. However, clear petrographic and sedimentologic evidence of glacial influence on deposition of the upper Urucum Formation, in which the in situ VSMs occur, favors

correlation with Cryogenian glacial episodes, thus showing that the record of VSMs, formerly thought to be exclusively Tonian in age, extends into Cryogenian periglacial marine settings. Indeed, recent sequence and chemostratigraphic analyses of the Jacadigo Group correlated the studied interval to the Marinoan cryochron. These findings call into question the use of the *Cycliocyrillium simplex* assemblage as a biostratigraphic tool for Tonian rocks.

## CRediT authorship contribution statement

**L. Morais:** Conceptualization, Data curation, Formal analysis, Writing - original draft. **B.T. Freitas:** Conceptualization, Data curation, Formal analysis, Supervision, Writing - original draft. **T.R. Fairchild:** Data curation, Formal analysis, Writing - original draft. **T.F. Toniolo:** Data curation, Formal analysis. **M.D.R. Campos:** Data curation, Formal analysis. **G.M.E.M. Prado:** Data curation, Formal analysis. **P.A.S. Silva:** Data curation, Formal analysis. **I.D. Rudnitzki:** Data curation. **D.J.G. Lahr:** Formal analysis. **J.M. Leme:** Project administration, Supervision. **P. Philippot:** Data curation, Formal analysis, Funding acquisition, Project administration. **M. Lopez:** Data curation, Formal analysis. **R.I.F. Trindade:** Data curation, Funding acquisition, Project administration, Supervision. All authors: Writing - review & editing.

## Declaration of Competing Interest

The authors declare that they have no known competing financial interests or personal relationships that could have appeared to influence the work reported in this paper.

## Acknowledgments

The authors thank the São Paulo Research Foundation (FAPESP) (grants #2015/16235-2; #2016/05937-9; #2016/06114-6; #2017/22099-0), CNPq (Conselho Nacional de Desenvolvimento Científico e Tecnológico) (grant 141861/2019-3), Eric Siciliano Rego for his help in samples selection, Vinicius Meira and Ticiano dos Santos for their help with detrital zircon geochronology, the mining company Vale for granting access to the drill core RAB-FD00019, and anonymous reviewers for their valuable suggestions. This study was financed in part by the Coordenação de Aperfeiçoamento de Pessoal de Nível Superior – Brasil (CAPES - Finance Code 001).

## Appendix A. Supplementary data

Supplementary data to this article can be found online at https://doi.org/10.1016/j.precamres.2021.106470.

## References

Almeida, F.F.M., 1945. Geologia do Sudoeste Matogrossense. Boletim da Divisão de Geologia e Mineralogia do Departamento Nacional de Produção Mineral 116, 1–118.

Almeida, F.F.M., 1946. Origem dos minérios de ferro e manganês de Urucum (Corumbá, Estado de Mato Grosso): Boletim da Divisão de Geologia e Mineralogia. DNPM, Rio de Janeiro.

Alvarenga, C.J.S., Oliveira, G.D., Vieira, L.C., Santos, R.V., Baptista, M.C., Dantas, E.L., 2019. Carbonate chemostratigraphy of the Vazante Group, Brazil: a probable Tonian age. Precambr. Res. 331, 105378. https://doi.org/10.1016/j.precamres.2019.105378.

Ananiadis, T., 1984. Petrographische und geochemische Untersuchungen der Bohrung Jacadigo PS-J-01, Urucum Distrikt, Mato Grosso do Sul, Brasilien, unter besonderer Berucksichtigung der grauen Silt-Sandstane. Thesis dissertation. Frankfurt University, p. 144 p..

Andersen, T., Elburg, M.A., Magwaza, B.N., 2019. Sources of bias in detrital zircon geochronology: Discordance, concealed lead loss and common lead correction. Earth Sci. Rev. 197, 102899. https://doi.org/10.1016/j.earscirev.2019.102899.

Angerer, T., Hagemann, S.G., Walde, D.H.G., Halverson, G.P., Boyce, A.J., 2016. Multiple metal sources in the glaciomarine facies of the Neoproterozoic Jacadigo iron formation in the "Santa Cruz deposit" Corumbá, Brazil. Precambr. Res. 275, 369–393.

Angerer, T., Hagemann, S.G., Walde, D.H.G., 2021. Diagenetic and supergene ore forming processes in the iron formation of the Neoproterozoic Jacadigo Group, Corumbá, Brazil. J. South Am. Earth Sci. 105, 102902 https://doi.org/10.1016/j.jsames.2020.102902.

Babinski, M., Boggiani, P.C., Trindade, R.I.F., Fanning, C.M., 2013. Detrital zircon ages and geochronological constraints on the Neoproterozoic Puga diamictites and associated BIFs in the southern Paraguay Belt, Brazil. Gondwana Res. 23, 988–997.

Barbosa, A.L.M., Oliveira, M.M.,1978, Ambientes de sedimentação do Grupo Jacadigo em Mato Grosso do Sul, Brasil, e no leste da Bolívia. Anais do Congresso Brasileiro de Geologia 30, vol. 2, p. 729-742.

Bloeser, B., 1985. *Melanocyrillium*, a new genus of structurally complex late Proterozoic microfossils from the Kwagunt Formation (Chuar Group), Grand Canyon, Arizona. J. Paleontol. 59, 741–765.

Chumakov, N.M., 2015. Problem of the identification of ancient glacial sediments. Lithol. Min. Resour. 50 (2), 134–143.

Cohen, P.A., Irvine, S.W., Strauss, J.V., Coxall, H., 2017. Vase-shaped microfossils from the Tonian Callison Lake Formation of Yukon, Canada: taxonomy, taphonomy and stratigraphic palaeobiology. Palaeontology 60 (5), 683–701.

Cook, J., Edwards, A., Takeuchi, N., Irvine-Fynn, T., 2016. Cryoconite: the dark biological secret of the cryosphere. Prog. Phys. Geogr. 40 (1), 66–111.

Corsetti, F.A., Awramik, S.M., Pierce, D., 2003. A complex microbiota from snowball Earth times: microfossils from the Neoproterozoic Kingston Peak Formation, Death Valley, USA. Proc. Natl. Acad. Sci. 100 (8), 4399–4404.

Cowan, E.A., Christoffersen, P., Powell, R.D., 2012. Sedimentological signature of a deformable bed preserved beneath an ice stream in a Late Pleistocene glacial sequence, Ross Sea, Antarctica. J. Sediment. Res. 82 (4), 270–282.

D'el-Rey, L.J.H., Walde, D.-G., Saldanha, D.O., 2016. The Neoproterozoic - Cambrian Paraguay Belt, central Brazil: Part I - new structural data and a new approach on the regional implications. Tectonophysics 676, 20–41.

Domack, E.W., Jacobson, E.A., Shipp, S., Anderson, J.B., 1999. Late Pleistocene-Holocene retreat of the West Antarctic Ice-Sheet system in the Ross Sea: Part 2 - sedimentologic and stratigraphic signature. Geol. Soc. Am. Bull. 111 (10), 1517–1536.

Dorr, J.V.N., 1945. Manganese and iron deposits of Morro do Urucum, Mato Grosso, Brazil. In: Bulletin of the United States Geological Survey, p. 47.

Dott Jr., R.H., 1964. Wacke, greywacke and matrix—what approach to immature sandstone classification? J. Sediment. Petrol. 34, 625–632.

Ewetz, C.E., 1933. Einige neue Fossilfunde in der Visingsöformation (Some new fossil finds in the Visingsö Formation): Geol. Fören. Stockh. Förh. 55 (3), 506–518.

Fairchild, T.R., Barbour, A.P., Haralyi, N.L.E., 1978. Microfossils in the "Eopaleozoic" Jacadigo Group at Urucum, Mato Grosso, Southwest Brazil. Boletim IG-USP 9, 74. https://doi.org/10.11606/issn.2316-8978.v9i0p74-79.

Frei, R., Døssing, L.N., Gaucher, C., Boggiani, P.C., Frei, K.M., Árting, T.B., Freitas, B.T., 2017. Extensive oxidative weathering in the aftermath of a late Neoproterozoic glaciation - Evidence from trace element and chromium isotope records in the Urucum district (Jacadigo Group) and Puga iron formations (Mato Grosso do Sul, Brazil). Gondwana Res. 49, 1–20.

Freitas, B.T., Warren, L.V., Boggiani, P.C., De Almeida, R.P., Piacentini, T., 2011. Tectono-sedimentary evolution of the Neoproterozoic BIF-bearing Jacadigo Group, SW-Brazil. Sed. Geol. 238 (1-2), 48–70.

Freitas, B.T., Rudnitzki, I.D., Morais, L., Campos, M.D.R., Almeida, R.P., Warren, L.V., Boggiani, P.C., Caetano-Filho, S., Bedoya-Rueda, C., Babinski, M., Fairchild, T.R., Trindade, R.I.F., 2021. Cryogenian glaciostatic and eustatic fluctuations and massive Marinoan-related deposition of Fe and Mn in the Urucum district. Brazil, Geology,. https://doi.org/10.1130/G49134.1.

Götze, J., Plötze, M., Götte, T., Neuser, R., Richter, D.K., 2002. Cathodoluminescence (CL) and electron paramagnetic resonance (EPR) studies of clay minerals. Mineral. Petrol. 76, 195–212.

Green, J.W., Knoll, A.H., Swett, K., 1988. Microfossils from oolites and pisolites of the Upper Proterozoic Eleonore Bay Group, central east Greenland. J. Paleontol. 62 (6), 835–852.

Hart, J.K., 2017. Subglacial till formation: microscale processes within the subglacial shear zone. Quat. Sci. Rev. 170, 26–44.

Hawes, I., Jungblut, A.D., Matys, E.D., Summons, R.E., 2018. The "Dirty Ice" of the McMurdo Ice Shelf: analogues for biological oases during the Cryogenian. Geobiology 16 (4), 369–377.

Hodson, A., Cameron, K., Bøggild, C., Irvine-Fynn, T., Langford, H., Pearce, D., Banwart, S., 2010. The structure, biological activity and biogeochemistry of cryoconite aggregates upon an Arctic valley glacier: Longyearbreen, Svalbard. J. Glaciol. 56 (196), 349–362.

Hoffman, P.F., 2016. Cryoconite pans on Snowball Earth: supraglacial oases for Cryogenian eukaryotes? Geobiology 14 (6), 531–542.

Hoffman, P.F., Abbot, D.S., Ashkenazy, Y., Benn, D.I., Brocks, J.J., Cohen, P.A., Cox, G.M., Creveling, J.R., Donnadieu, Y., Erwin, D.H., Fairchild, I.J., Ferreira, D., Goodman, J.C., Halverson, G.P., Jansen, M.F., Le Hir, G., Love, G.D., Macdonald, F.A., Maloof, A.C., Partin, C.A., Ramstein, G., Rose, B.E.J., Rose, C.V., Sadler, P.M., Tziperman, E., Voigt, A., Warren, S.G., 2017. Snowball Earth climate dynamics and Cryogenian geology-geobiology. Sci. Adv. 3 (11), e1600983.

Hiemstra, J.F., Van Der Meer, J.J.M., 1997. Pore-water controlled grain fracturing as an indicator for subglacial shearing in tills. J. Glaciol. 43 (145), 446–454.

Hiemstra, J.F., Rijsdijk, K.F., 2003. Observing artificially induced strain: implications for subglacial deformation. J. Quat. Sci. 18 (5), 373–383.

Hiemstra, J.F., Rijsdijk, K.F., Evans, D.J.A., Van Der Meer, J.J.M., 2005. Integrated micro-and macro-scale analyses of Last Glacial Maximum Irish Sea Diamicts from Abermawr and Traeth y Mwnt, Wales, UK. Boreas 34 (1), 61–74.

Kilfeather, A.A., Ó Cofaigh, C., Dowdeswell, J.A., van der Meer, J.J.M., Evans, D.J.A., 2010. Micromorphological characteristics of glacimarine sediments: implications for distinguishing genetic processes of massive diamicts. Geo-Mar. Lett. 30 (2), 77–97.

Kluiving, S.J., Bartek, L.R., van der Wateren, F.M., 1999. Multi-scale analyses of subglacial and glaciomarine deposits from the Ross Sea continental shelf, Antarctica. Ann. Glaciol. 28, 90–96.
Knoll, A.H, 1996, Archean and Proterozoic paleontology in Palynology: Principles and Applications, Jansonius. Jansonius, J., McGregor, D.C. (Eds.), 1. American Association of Stratigraphic Palynologists Foundation, pp. 51-80.
Knoll, A.H., Javaux, E.J., Hewitt, D., Cohen, P., 2006. Eukaryotic organisms in Proterozoic oceans. Philos. Trans. R. Soc. B Biol. Sci. 361 (1470), 1023–1038.
Knoll, A.H., Calder, S., 1983. Microbiotas of the Late Precambrian Ryssö Formation, Nordaustlandet, Svalbard. Palaeontology 26, 467–496.
Knoll, A.H., Vidal, G., 1980. Late Proterozoic vase-shaped microfossils from the Visingsö Beds, Sweden. Geologiska Föreningen I Stockholm Förhandlingar 102 (3), 207–211.
Knoll, A.H., Swett, K., Burkhardt, E., 1989. Paleoenvironmental distribution of microfossils and stromatolites in the Upper Proterozoic Backlundtoppen Formation, Spitsbergen. J. Paleontol. 63 (2), 129–145.
Knoll, A.H., Swett, K., Mark, J., 1991. Paleobiology of a Neoproterozoic tidal flat/lagoonal complex: the Draken Conglomerate Formation, Spitsbergen. J. Paleontol. 65 (4), 531–570.
Lacerda Filho, J.W., Brito, R.S.C., Silva, M.G., de Oliveira, C.C., Moreton, L.C., Martins, E. G., Lopes, R.C., Lima, T.M., Larizzatti, J.H., Valente, C.R., 2006. In: Geologia e Recursos Minerais do Estado de Mato Grosso do Sul. Programa integração, atualização e difusão de dados de geologia do Brasil. Convênio CPRM/SICME - MS, MME, p. 28 p..
Lechte, M.A., Wallace, M.W., van Smeerdijk Hood, A., Li, W., Jiang, G., Halverson, G.P., Asael, D., Mc Coll, A.L., Planavsky, N.J., 2019. Subglacial meltwater supported aerobic marine habitats during Snowball Earth. Proc. Natl. Acad. Sci. 116 (51), 25478–25483.
Lisboa, M.A.R., 1909, Oeste de São Paulo, Sul de Mato Grosso; geologia, indústria mineral, clima, vegetação, solo agrícola, indústria pastoril. Rio de Janeiro, TYP. do Jornal do Commercio, 172 p.
Martí Mus, M., 2001. Palaeobiology and taphonomy of early problematic fossil. Ph.D dissertation. Uppsala University.
Martí Mus, M., Moczydowska, M., 2000. Internal morphology and taphonomic history of the Neoproterozoic vase-shaped microfossils from the Visingsö Group, Sweden. Norsk Geologisk Tidsskrift 80 (3), 213–228.
Mazumder, A., Govil, P., Kar, R., Gayathri, N.M., Raghuram, 2017. Paleoenvironments of a proglacial lake in Schirmacher Oasis, East Antarctica: insights from quartz grain microtextures. Pol. Polar Res. 38, 1–19.
McGee, B., Babinski, M., Trindade, R., Collins, A.S., 2018. Tracing final Gondwana assembly: Age and provenance of key stratigraphic units in the southern Paraguay Belt, Brazil. Precambr. Res. 307, 1–33.
Meer, J.J. van der, 1993. Microscopic evidence of subglacial deformation. Quat. Sci. Rev. 12 (7), 553–587.
Menzies, J., Meer, J.J.M., 2018. Micromorphology and microsedimentology of glacial sediments. In: Past Glacial Environments. Elsevier, pp. 753–806. https://doi.org/10.1016/B978-0-08-100524-8.00036-1.
Moczydłowska, M., Pease, V., Willman, S., Wickström, L., Agić, H., 2017. A Tonian age for the Visingsö Group in Sweden constrained by detrital zircon dating and biochronology: implications for evolutionary events. Geol. Mag. 155 (5), 1175–1189.
Morais, L., Fairchild, T.R., Lahr, D.J.G., Rudnitzki, I.D., Schopf, J.W., Garcia, A.K., Kudryavtsev, A.B., Romero, G.R., 2017. Carbonaceous and siliceous Neoproterozoic vase-shaped microfossils (Urucum Formation, Brazil) and the question of early protistan biomineralization. J. Paleontol. 91 (3), 393–406.
Morais, L., Lahr, D.J.G., Rudnitzki, I.D., Freitas, B.T., Romero, G.R., Porter, S.M., Knoll, A.H., Fairchild, T.R., 2019. Insights into vase-shaped microfossil diversity and Neoproterozoic biostratigraphy in light of recent Brazilian discoveries. J. Paleontol. 93 (4), 612–627.
Navarro, M.S., Tonetto, E.M., Oliveira, E.P., 2017. Peixe zircon: new Brazilian reference material for U-Pb geochronology by LA-SF-ICP MS. Goldschmidt Conference. Presented at the Goldschmidt Conference.
Navarro, M.S., Tonetto, E.M., Oliveira, E.P., 2015, LA-SF-ICP-MS U-Pb zircon dating at University of Campinas, Brazil, In: IAG, Geoanalysis. Presented at the IAG, Geoanalysis, p. 86.
Okamura, T., Nishido, H., Ninagawa, K., Sakamoto, T., 2006. Cathodoluminescence and thermoluminescence studies of clay minerals. Clay Sci. 11, 59–68.
Paton, C., Woodhead, J.D., Hellstrom, J.C., Hergt, J.M., Greig, A., Maas, R., 2010. Improved laser ablation U-Pb zircon geochronology through robust downhole fractionation correction: Geochemistry. Geophys., Geosyst. 11 (3), n/a–n/a.
Piacentini, T., Vasconcelos, P.M., Farley, K.A., 2013. $^{40}Ar/^{39}Ar$ constraints on the age and thermal history of the Urucum Neoproterozoic banded iron-formation, Brazil. Precambr. Res. 228, 48–62.
Phillips, E., Merritt, J., Auton, C., Golledge, N., 2007. Microstructures in subglacial and proglacial sediments: understanding faults, folds and fabrics, and the influence of water on the style of deformation. Quat. Sci. Rev. 26 (11-12), 1499–1528.
Piotrowski, J.A., Larsen, N.K., Menzies, J., Wysota, W., 2006. Formation of subglacial till under transient bed conditions: deposition, deformation, and basal decoupling under a Weichselian ice sheet lobe, central Poland. Sedimentology 53 (1), 83–106.
Porter, S.M., Meisterfeld, R., Knoll, A.H., 2003. Vase-shaped microfossils from the Neoproterozoic Chuar Group, Grand Canyon: a classification guided by modern testate amoebae. J. Paleontol. 77 (3), 409–429.
Redes, L.A., Sousa, M.Z.A., Ruiz, A.S., Lafon, J.M., 2015. Petrogenesis and U-Pb and Sm-Nd geochronology of the Taquaral granite: record of an Orosirian continental magmatic arc in the region of Corumbá – MS. Braz. J. Geol. 45 (3), 431–451.
Riedman, L.A., Porter, S.M., Calver, C.R., 2018. Vase-shaped microfossil biostratigraphy with new data from Tasmania, Svalbard, Greenland, Sweden and the Yukon. Precambr. Res. 319, 19–36.
Runkel, A.C., Mackey, T.J., Cowan, C.A., Fox, D.L., 2010. Tropical shoreline ice in the late Cambrian: Implications for Earth's climate between the Cambrian Explosion and the Great Ordovician Biodiversification Event. GSA Today 4–10. https://doi.org/10.1130/GSATG84A.110.1130/2010290.
Saito, Y., Tiba, T., Matsubara, S., 1988. Precambrian and Cambrian cherts in north-western Tasmania. Bull. Natl. Sci. Museum Tokyo, Series C 14 (2), 59–70.
Sergeev, V.N., Schopf, J.W., 2010. Taxonomy, paleoecology and biostratigraphy of the late Neoproterozoic Chichkhan microbiota of South Kazakhstan: the marine biosphere on the eve of metazoan radiation. J. Paleontol. 84, 363–401.
Schopf, J.W., 1992. Evolution of the Proterozoic biosphere: benchmarks, tempo, and mode. In: Schopf, J.W., Klein, C. (Eds.), The Proterozoic Biosphere: A Multidisciplinary Study. Cambridge University Press, pp. 585–600.
Schmitz, M.D., Schoene, B., 2007. Derivation of isotope ratios, errors, and error correlations for U-Pb geochronology using $^{205}Pb$-$^{235}U$-($^{233}U$)-spiked isotope dilution thermal ionization mass spectrometric data: Geochemistry. Geophys., Geosyst. 8 (8), n/a–n/a. https://doi.org/10.1029/2006GC001492.
Smith, E.F., Macdonald, F.A., Crowley, J.L., Hodgin, E.B., Schrag, D.P., 2015. Tectonostratigraphic evolution of the c. 780–730 Ma Beck Spring Dolomite: basin formation in the core of Rodinia. In: Li, Z.X., Evans, D.A.D., Murphy, J.B. (Eds.), Supercontinent Cycles Through Earth History, Geological Society, London, Special Publications, p. 213.
Spencer, C.J., Kirkland, C.L., Taylor, R.J.M., 2016. Strategies towards statistically robust interpretations of in situ U-Pb zircon geochronology. Geosci. Front. 7 (4), 581–589.
Strauss, J.V., Rooney, A.D., Macdonald, F.A., Brandon, A.D., Knoll, A.H., 2014. 740 Ma vase-shaped microfossils from Yukon, Canada: Implications for Neoproterozoic chronology and biostratigraphy. Geology 42 (8), 659–662.
Sweet, D.E., Brannan, D.K., 2016. Proportion of glacially to fluvially induced quartz grain microtextures along the Rhitina river, SE Alaska, USA. J. Sedimentary Res. 86, 749–761.
Takeuchi, N., Nishiyama, H., Li, Z., 2010. Structure and formation process of cryoconite granules on Urumqi glacier No.1, Tien Shan, China. Ann. Glaciol. 51 (56), 9–14.
Trompette, R., de Alvarenga, C.J.S., Walde, D., 1998. Geological evolution of the Neoproterozoic Corumbá graben system (Brazil): depositional context of the stratified Fe and Mn ores of the Jacadigo Group. J. S. Am. Earth Sci. 11 (6), 587–597.
Urban, H., Stribrny, B., Lippolt, H.J., 1992. Iron and manganese deposits of the Urucum district Mato Grosso do Sul, Brazil. Econ. Geol. 87, 1375–1392.
Vermeesch, P., 2018. IsoplotR: A free and open toolbox for geochronology. Geosci. Front. 9 (5), 1479–1493.
Vermeesch, P., 2021. On the treatment of discordant detrital zircon U-Pb data. Geochronology 3, 247–257.
Vidal, G., 1979. Acritarchs from the upper Proterozoic and lower Cambrian of East Greenland. Grønlands Geologiske Undersøgelse 134, 1–55.
Walde, D.H.G., Gierth, E., Leonardos, O.H., 1981. Stratigraphy and mineralogy of the manganese ores of Urucum, Mato Grosso, Brazil. Geol. Rundschau 70 (3), 1077–1085.
Waller, R., Murton, J., Whiteman, C., 2009. Geological evidence for subglacial deformation of Pleistocene permafrost. Proc. Geol. Assoc. 120 (2-3), 155–162.
Weiss, M.P., Sweet, W.C., 1959, Stratigraphy and structure of the Mutun Mountains, Department of Santa Cruz, Bolivia, Congreso Geológico Internacional, XX Sesión, Ciudad de México, Seccioón XIII, Geología Aplicada a la Ingeniería y a la Minería, pp. 399-413.
Wiedenbeck, M., Alle, P., Corfu, F., Griffin, W.L., Meier, M.M., Oberli, F.A., Von Quadt, A., Roddick, J.C., Spiegel, W., 1995. Three natural zircon standards for U-Th-Pb Lu-Hf, trace element and REE analyses. Geostand. Newsl. 19 (1), 1–23.
Woese, C.R., Kandler, O., Wheelis, M.L., 1990. Towards a natural system of organisms: proposal for the domains Archaea, Bacteria and Eucarya. Proc Natl. Acad. Sci. 87 (12), 4576–4579.
Woronko, B., Pisarska-Jamroży, M., 2016. Micro-scale frost weathering of sand-sized quartz grains. Permafrost Periglac. Process. 27 (1), 109–122.
Yang, M., Frank, T.D., Fielding, C.R., 2018. Cryogenic brine and its impact on diagenesis of glaciomarine deposits, McMurdo Sound, Antarctica. J. Sedimentary Res. 88, 898–916.